Supplementary Information: A spectroscopic description of the E_1 state of Mo Nitrogenase based on Mo and Fe X-ray absorption and Mössbauer studies

Casey Van Stappen[†], Roman Davydov[‡], Zhi-Yong Yang[§], Ruixi Fan[⊥], Yisong Guo[⊥], Eckhard Bill[†], Lance C. Seefeldt[§], Brian M. Hoffman[‡], Serena DeBeer*[†]

[†]Max Planck Institute for Chemical Energy Conversion, Stiftstr. 34-36, 45470 Mülheim a. d. Ruhr, Germany
email: serena.debeer@cec.mpg.de
[§]Department of Chemistry and Biochemistry, Utah State University, Logan UT, 84322
[‡]Department of Chemistry, Northwestern University, Evanston IL, 60208
[⊥]Department of Chemistry, Carnegie Mellon University, Pittsburgh PA, 15213

Table of Contents

1. Preparation of Model Complexes

General considerations:

Model complexes $Mo^{III}Cl_3(thf)_3$, $Mo^{III}Cl_3ttcn$, and $[NEt_4][TpMo^{IV}S_4S]$ were synthesized according to previously established procedure.[1-3] Unless indicated otherwise, all reactions were conducted using oven-dried glassware in a nitrogen-filled glovebox or on a Schlenk line using standard Schlenk techniques. THF was purchased anhydrous from Sigma, vacuum distilled from sodium benzophenone ketyl and stored over 4 Å molecular sieves prior to use. Elemental analysis was conducted by Mikrolab Kolbe (Mülheim an der Ruhr, Germany). Unless indicated otherwise, all reagents were purchased from commercial sources and used as received. 1,4,7-trithiacyclonane was purchased from Sigma. $MoCl_3(thf)_3$ and $TpMoS_4S$ were prepared according to literature procedure.[1-2]

2. EPR

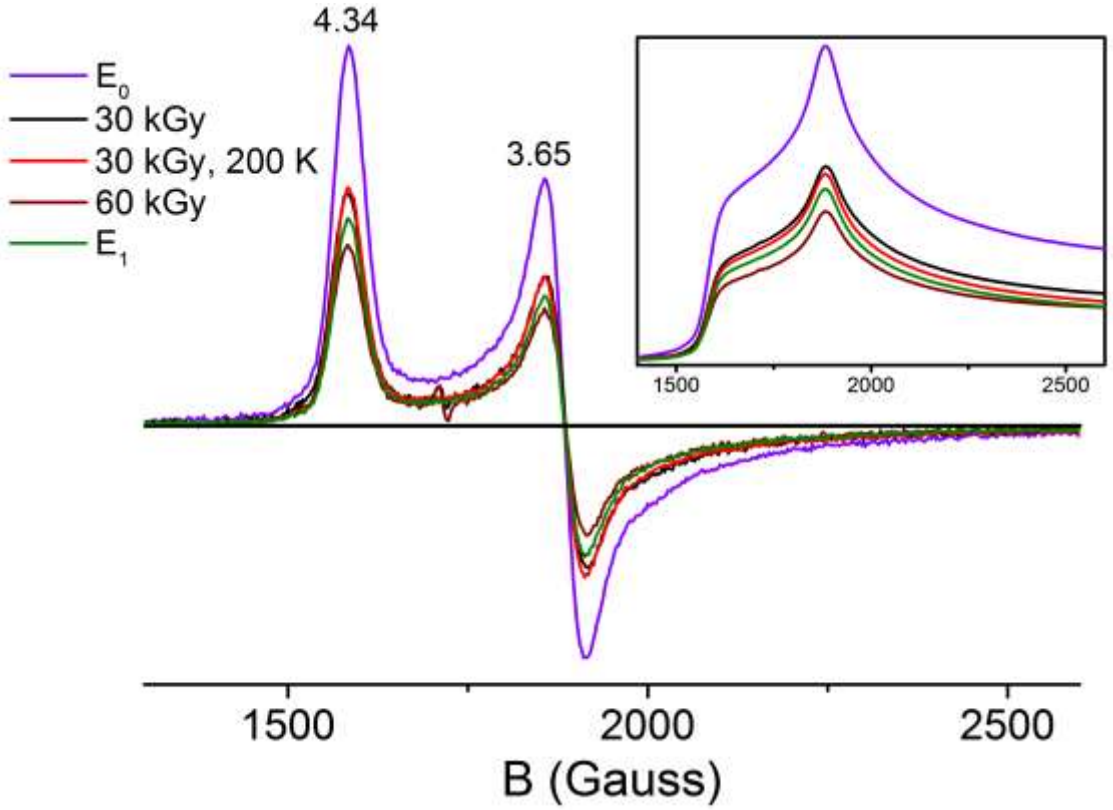

Figure S1. EPR spectra of g_1, g_2 (4.34, 3.65, respectively) of the S = 3/2 of resting E_0 MoFe and reduced samples. Measurements were performed directly for samples contained in X-ray cuvettes and used for subtraction in XAS measurements to generate hypothetical pure spectra. The $g \sim 2$ region is not shown as irradation of the Delrin® plastic XAS cells generates large radical signals, which obscure this part of the spectrum. EPR measurements were using a continuous wave (cw) X-band EPR spectra were recorded on a Bruker E500 ELEXSYS spectrometer equipped with a Bruker dual-mode cavity (ER4116DM) and an Oxford Instruments helium flow cryostat (ESR 900). A high-sensitivity Bruker Super-X (ER-049X) bridge with integrated microwave frequency counter was employed as the microwave unit. A magnetic field controller (ER032T) was externally calibrated with a Bruker NMR field probe (ER035M). Measurements were recorded at temperatures of 10 K using 2 mW microwave power and 7.5 G/100 kHz modulation.

Table S1. Percent reduction of the S=3/2 signal of E_0 observed in native and cryoreduced samples as determined by g_1 and peak height at g = 3.65/B = 1880 G of the absorption spectrum. The values from column g_1 were used to remove E_0 from the presented XAS spectra.

	Quantification method	
Sample	g_1	Integrated peak height
E_0	0%	0%
30 kGy	37%	38 %
30 kGy, 200 K annealed	39%	41 %
60 kGy	52%	52 %
50:1 MoFe:FeP native	44%	46 %

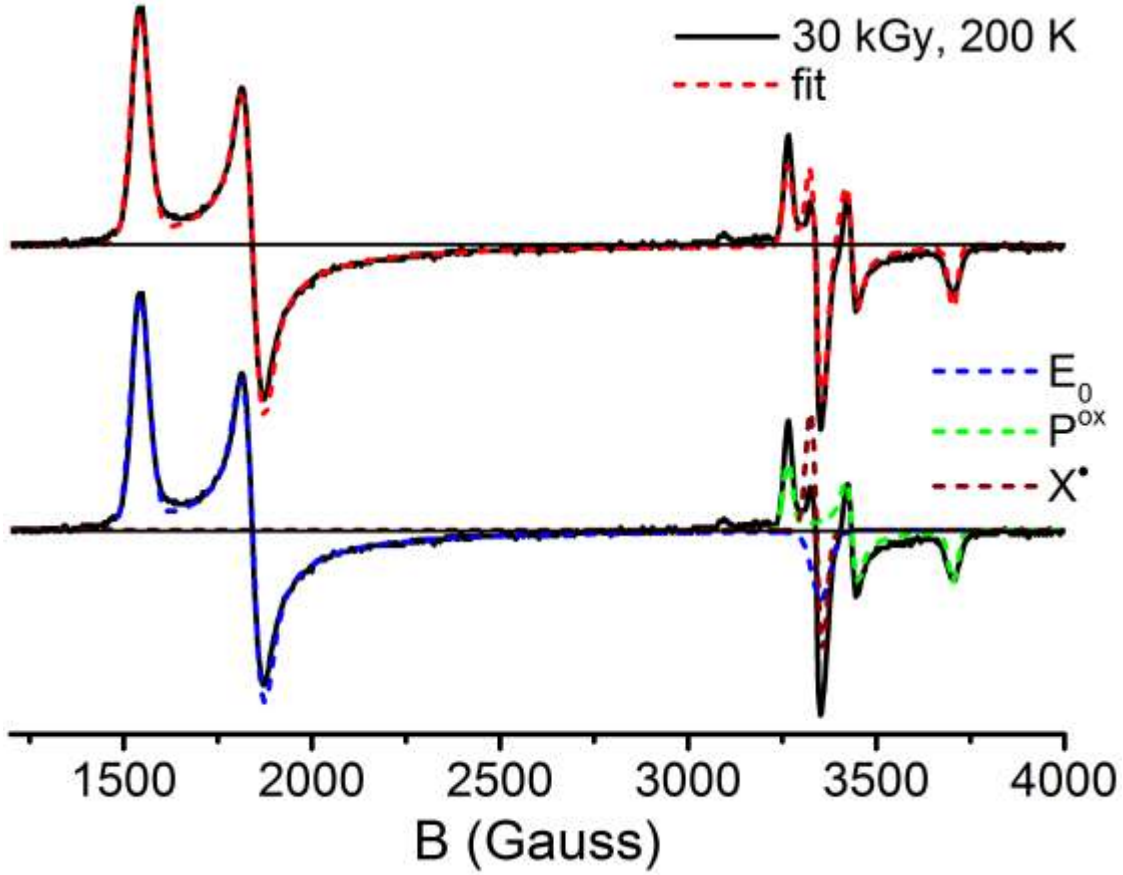

Figure S2. Simulation of the X-band EPR spectrum of cryoreduced/annealed MoFe (30 kGy, 200 K). Three contributions are required to model this spectrum, namely the $S = {}^3/_2$ E_0 component, the $S = {}^1/_2$ P^{1+} component, and an additional $S = {}^1/_2$ radical ($X^{\bullet}$). Measurement of 30 kGy, 200 K was performed at 10 K, 9.371 GHz using a power of 2 mW and a 13 G modulation amplitude. While several $S = {}^5/_2$ P^{1+} signals (g ~ 7.3,6.67,5.3) have been previously reported,[4] none are observed presently; simulation of these signals at quantities within the level of noise of the experiment lead to <1% contribution to the estimated final concentration of P^{1+}.

Table S2. EPR fit components of the simulation of the 30 kGy, 200 K. Spin quantification of each component is based on double-integration. The values given for each correction are compounded from left-to-right, meaning the provided AV corr. values have already had the k_B corr. applied, and both k_B corr. and AV corr. have been incorporated into the [MoFe] corr. values. [MoFe] corr. provides the final estimated concentration of P^{1+} in all cryoreduced samples.

		Contribution			
Component	[g_1, g_2, g_3]	Raw	[a]k_B corr.	[b]AV corr.	[c][MoFe] corr.
E_0	4.33, 3.63, 2.00	92%	93%	87%	65%
P^{1+}	2.05, 1.95, 1.81	7%	6%	10%	7%
$X^{\bullet}$	2.00, 2.00, 2.00	1%	1%	1%	---

[a]k_B corr. accounts for the difference in Boltzmann population $M_S = {}^1/_2$ (85%) and $M_S = {}^3/_2$ (15%) levels of the $S = {}^3/_2$ manifold at 10 K; these calculations were performed using the previously determined estimate of the zero-field splitting paramaeters D = 6.0 cm^{-1} and E/D = 0.055.[5] [b]AV corr. uses the correction of Asaa and Vänngård[6] to properly scale the relative intensities based on their g-values. [c][MoFe] corr. rescales E_0 and P^{1+} contributions relative to the total concentration of MoFe present (as determined by the resting state EPR spectrum provided in Figure 1 of the main text); this is possible as Femoco and P-cluster are present in a known 1:1 ratio.

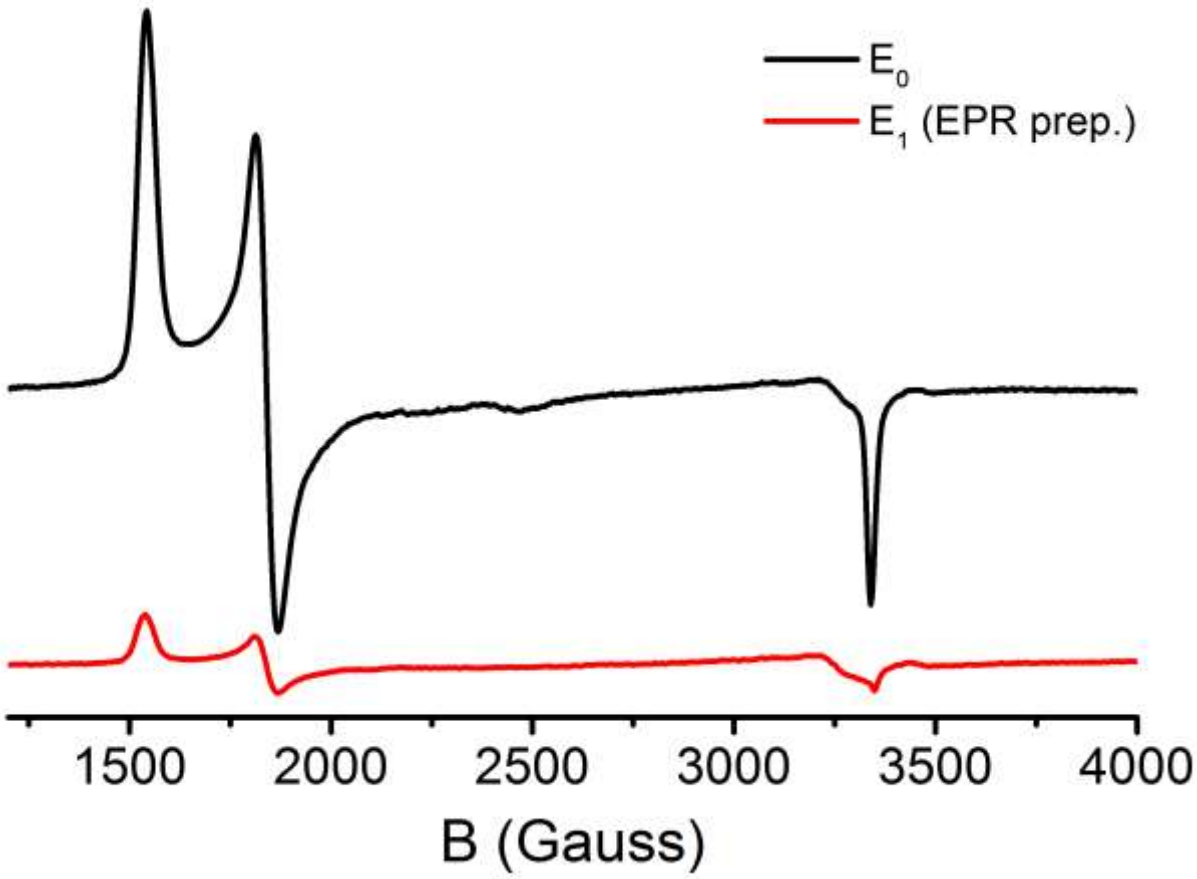

Figure S3. As an additional note, we found that native low-flux turnover (red) prepared in a quartz X-band EPR tube resulted in ~80% reduction in the S = $^3/_2$ signal of the E_0 state (black). This native turnover sample was prepared using 500 μM [MoFe], 8 μM [FeP], and quenched after 10 minutes reaction time. Measurements were performed at 10 K, 9.371 GHz using a power of 2 mW and a 13 G modulation amplitude.

3. Mo XAS

To provide insight into the possible changes which may occur upon reduction of the Mo center of MoFe, a series of model complexes were investigated. The normalized Mo Kα-HERFD XAS spectra of resting MoFe along with the $Mo^{III}Cl_3(thf)_3$, $Mo^{III}Cl_3$ttcn, and $TpMo^{IV}S_4S$ model complexes are shown in Figure S4. There is a clear decrease in the energy of the edge of -1 to -1.2 eV when comparing $TpMo^{IV}S_4S$ with MoFe, $Mo^{III}Cl_3(thf)_3$, and $Mo^{III}Cl_3$(ttcn). This is consistent with the decrease in effective nuclear charge experienced by valence shell which occurs upon reduction, matching our previous Mo Kα-HERFD measurements.[7] The pre-edge feature both loses intensity and shifts to lower energy when moving from Mo^{IV} to Mo^{III} as follows: $TpMo^{IV}S_4S$ (0.23 a.u., 20002.7 eV), MoFe (0.15 a.u., 20002.1 eV), $Mo^{III}Cl_3(thf)_3$ (0.09 a.u., 20001.5 eV), $Mo^{III}Cl_3$(ttcn) (0.06 a.u., 20001.5 eV). This feature is associated with the 1s $\rightarrow$ 4d transition which gains intensity through 4d-5p mixing. While the position of this feature is predominately impacted by effective nuclear charge, its relative intensity arises from several factors.[8-9] First, an increased d-count results in a decrease in the total number of d-holes available, which is manifested as a decrease in pre-edge intensity upon reduction. Additionally, the distribution of electrons in the d-manifold can directly impact the inherent symmetry of the Mo center through the Jahn-Teller distortion. For example, the $^3T_1$ electronic ground state of octahedral Mo^{IV} consists of two electrons occupying some combination of the d_{xy}, d_{xz}, or d_{yz}, and will undergo distortion to remove degeneracy. Meanwhile, the usual $^4A_2$ ground state of octahedral Mo^{III} is inherently symmetric and will not undergo distortion. Finally, the coordination environment can impact pre-edge intensity both through the local symmetry and covalency. Generally, an increase in symmetry will decrease 4d-5p mixing and thus a lower the observed pre-edge intensity. The pre-edge intensities of all Mo^{III} systems shown in Figure S4 are lower than that of $TpMo^{IV}S_4S$. It is also clear that as we increase the local symmetry imparted by the ligand environment from C_s (MoFe) to C_{2v} ($MoCl_3(thf)_3$) to C_{3v} ($MoCl_3$ttcn) the intensity of the pre-edge is greatly diminished. All of these results are in good agreement with previously observed trends of Mo Kα-HERFD XAS as a function of oxidation state.[7]

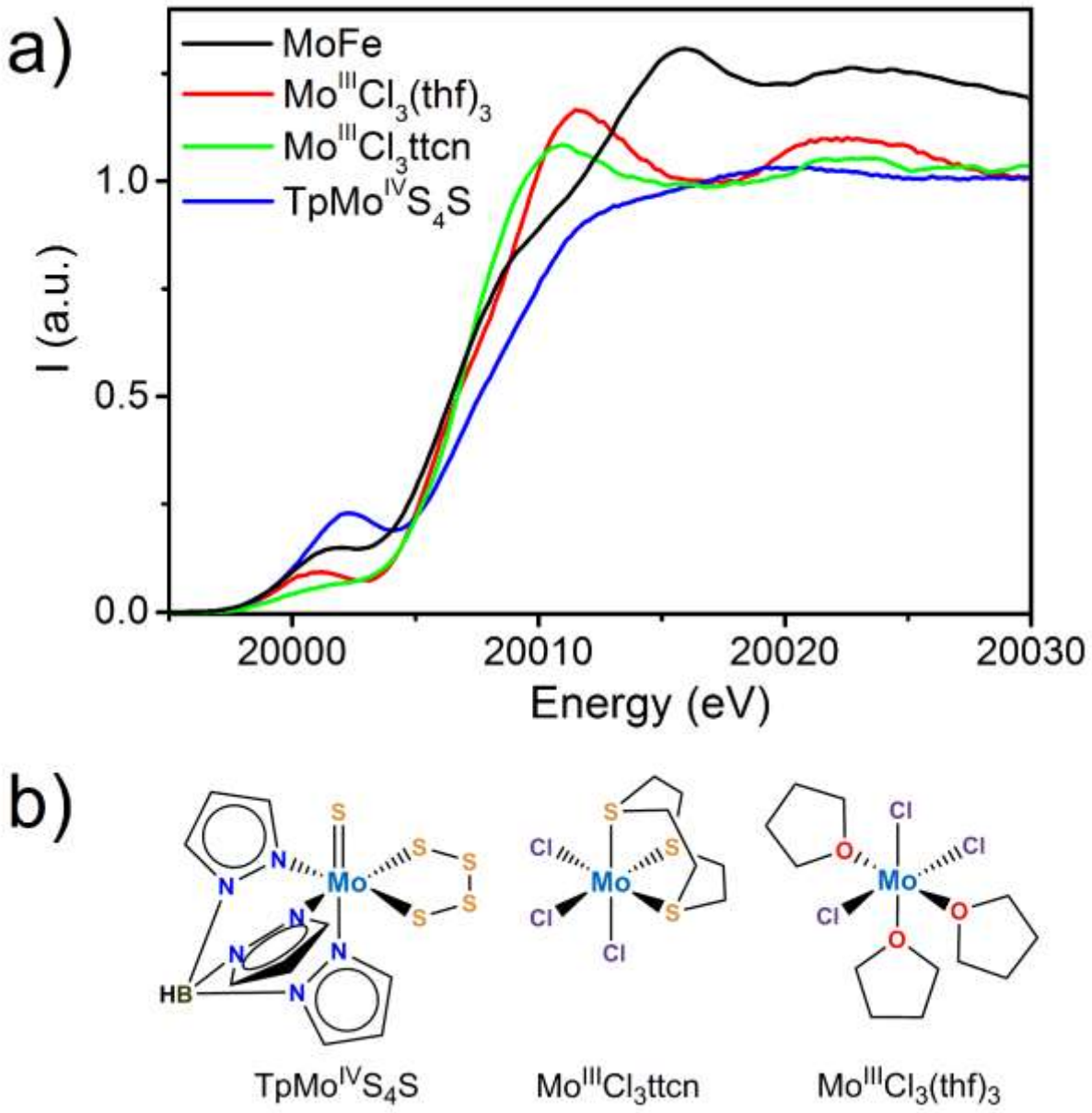

Figure S4. a) Normalized Mo Kα-HERFD XAS spectra of a series of b) Mo model complexes ([NEt_4][$TpMo^{IV}S_4S$], $Mo^{III}Cl_3ttcn$, and $Mo^{III}Cl_3(thf)_3$), along with resting Mo N2ase.[3] An 11-point boxcar average smoothing has been applied to the spectrum of MoFe.

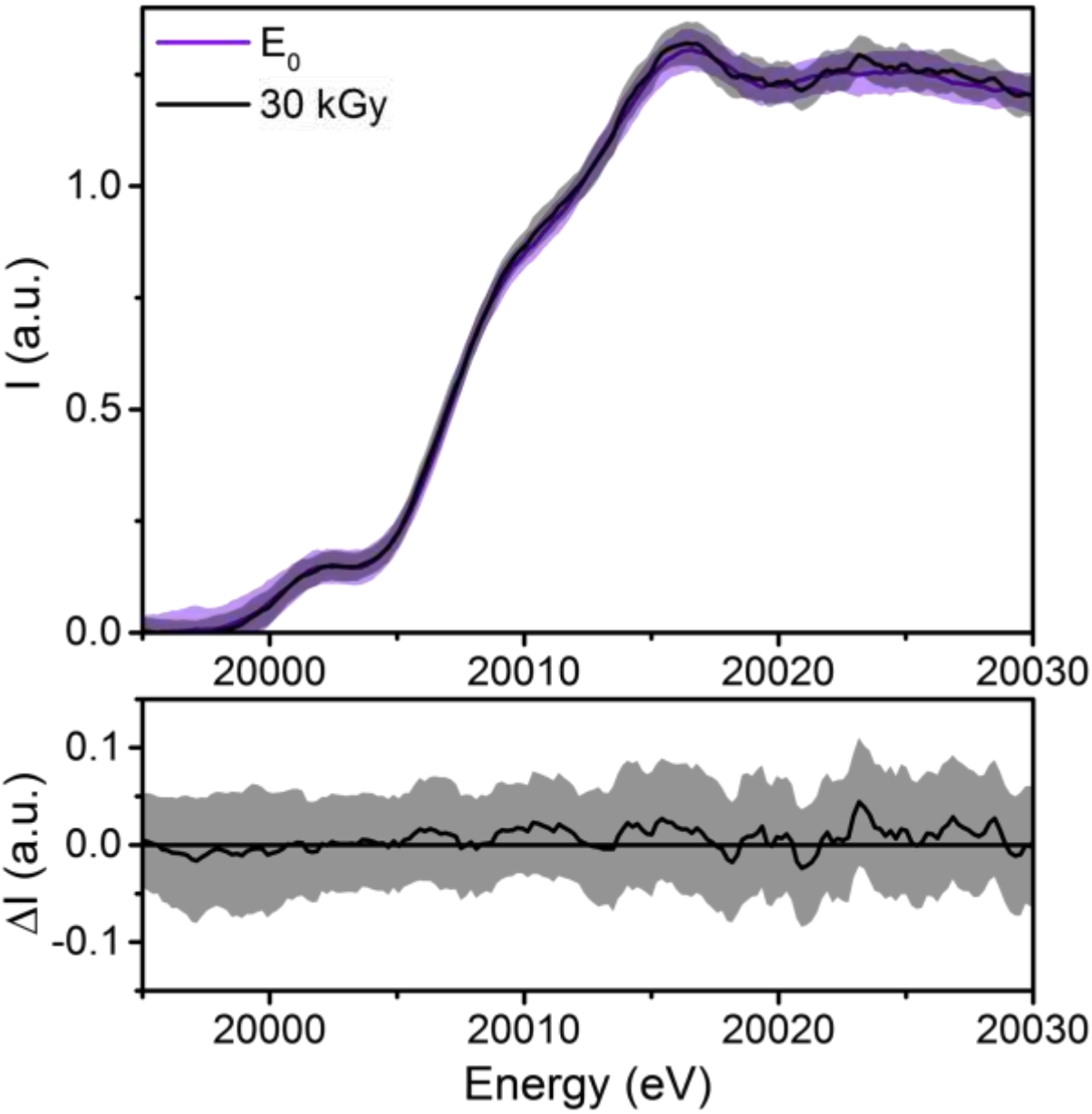

Figure S5. (top) Mo Kα-HERFD of resting E_0 and 30 kGy cryoreduced MoFe. Statistics were calculated according to equation 2 of the main text. An 11-point boxcar average was applied to the individual scans contributing to each averaged spectrum, and the calculated standard deviation shown are based upon individual scans which have undergone this averaging procedure. (bottom) Difference spectrum calculated by subtraction of E_0 from the 30 kGy spectrum, with standard error shown as the gray shaded area.

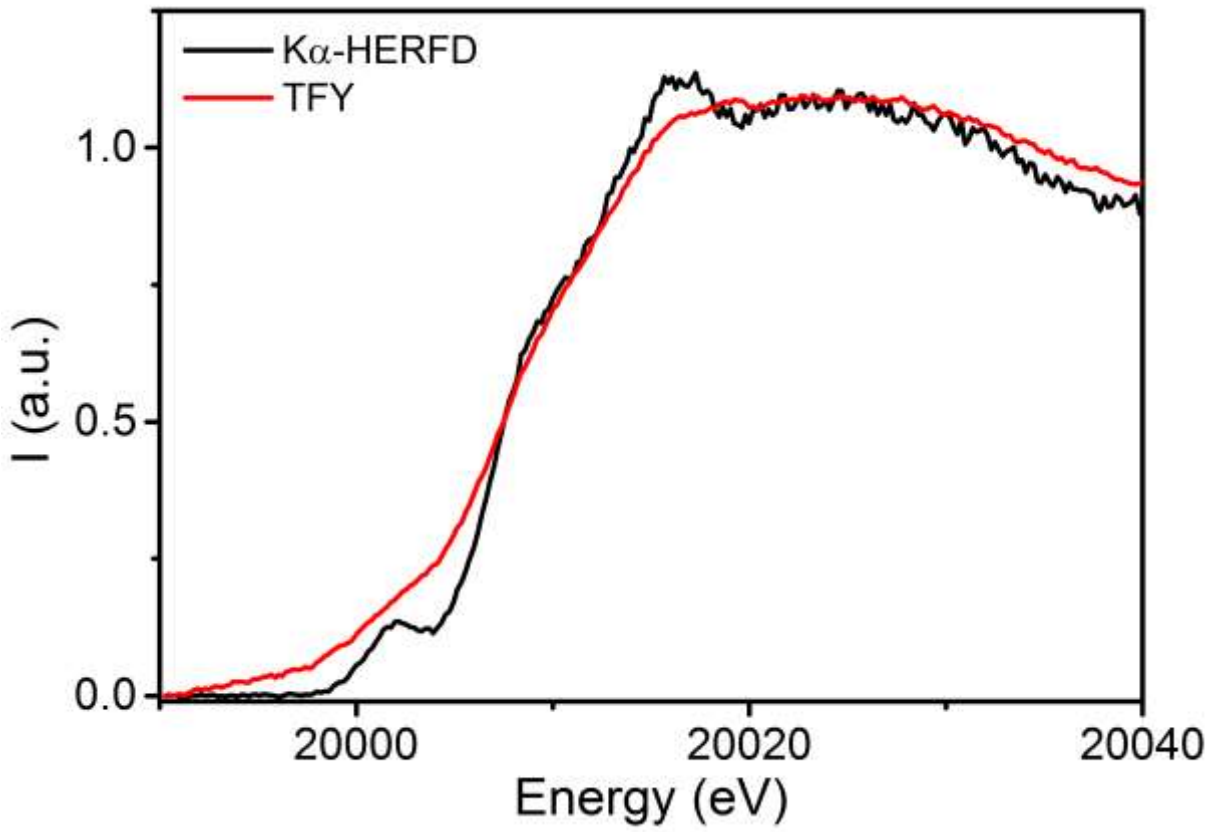

Figure S6. Mo K-edge of MoFe (E_0 state) demonstrating the improved line-width accomplished using HERFD (black) over total fluorescence yield (TFY) detection methods.

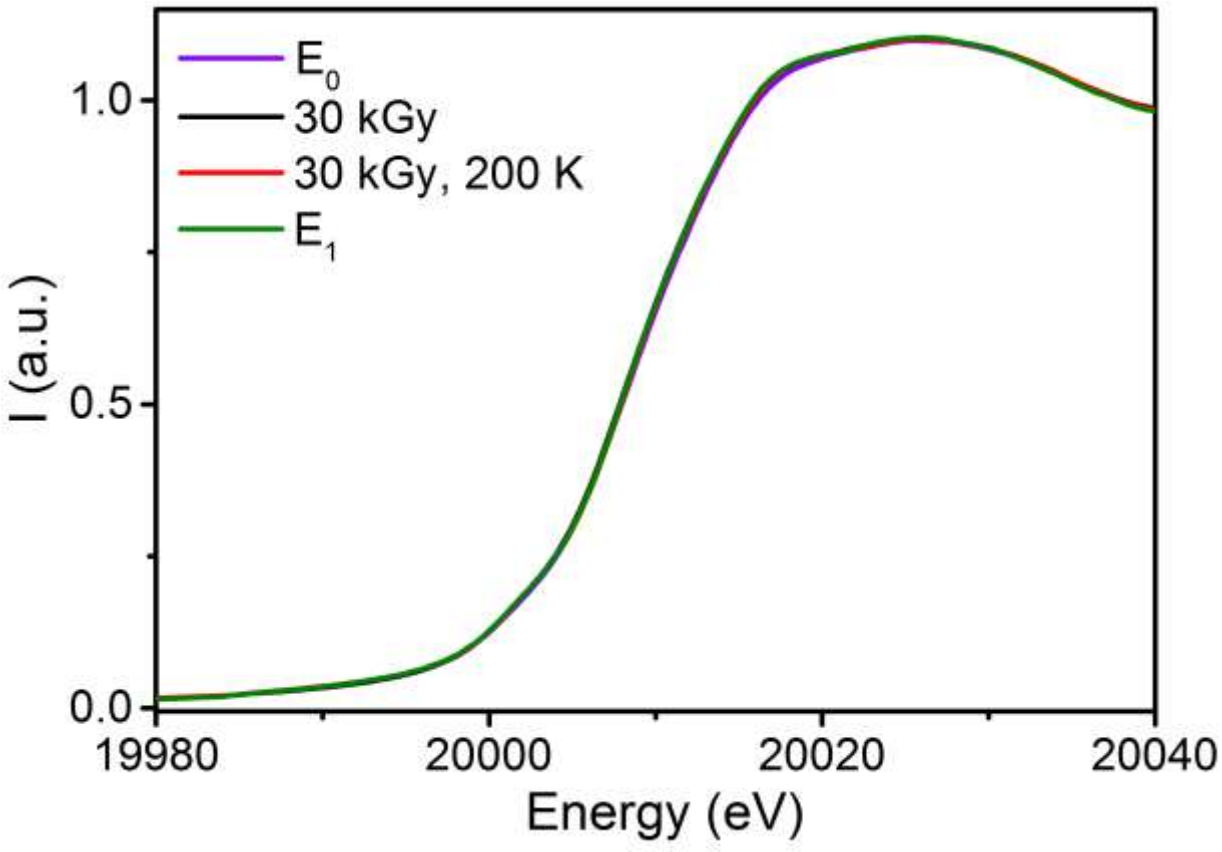

Figure S7. Mo K-edge PFY XAS spectra of resting and reduced MoFe species under investigation.

4. Fe XAS

The Fe Kα-HERFD of MoFe has been previously reported and discussed in detail,[10] and thus only briefly summarize the observed features and their origin here. The spectra exhibit two pre-edge features at 7112.8 eV and 7114.6 eV, an inflection in the rising edge at 7118.4 eV, and a broad white line feature ~7125 eV. The first pre-edge feature arises from the 1s → 3d transition, which, while formally dipole forbidden, gains intensity through C_{3v}-symmetry allowed 3d-4p mixing.[11-13] The second pre-edge feature has been attributed to the FeMoco cluster, and may arise from either a metal-to-ligand or more likely a metal-to-metal charge transfer transitions.[10]

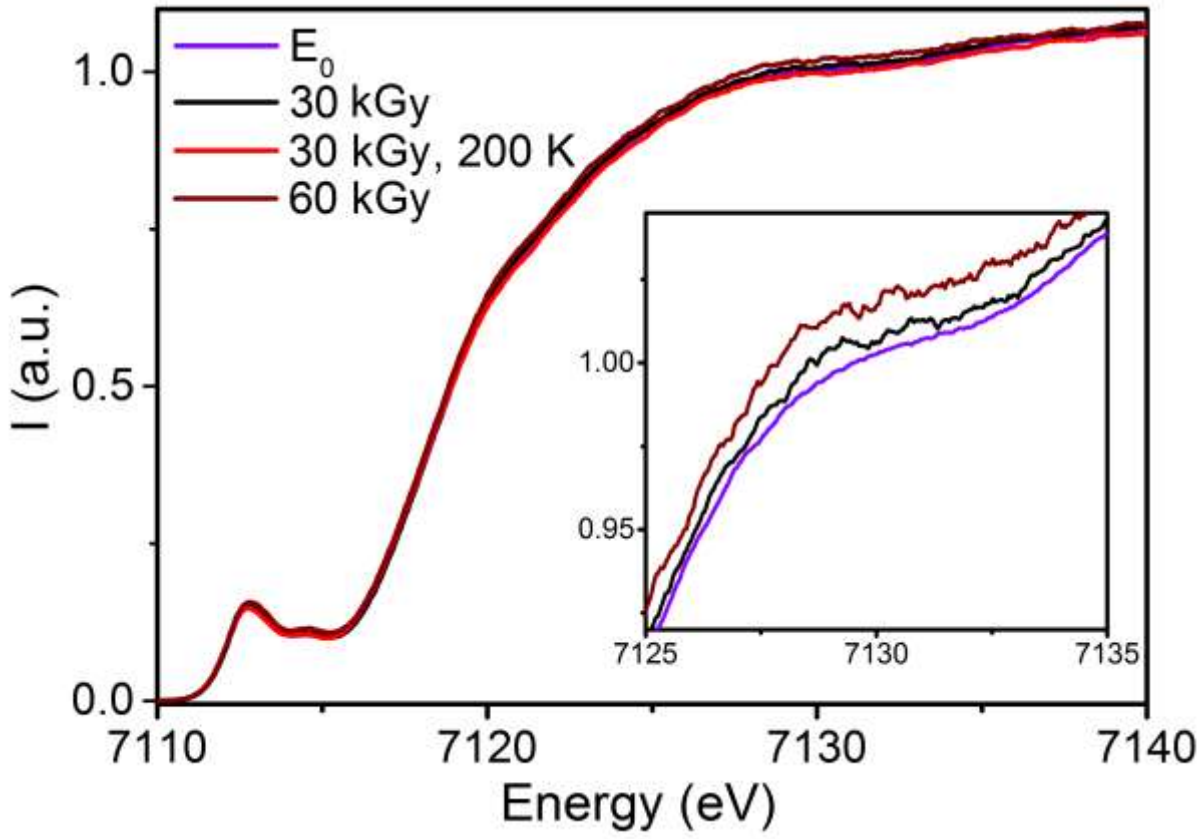

Figure S8. Fe Kα-HERFD of the cryoreduced series. The inset is limited to presenting the E_0, 30 kGy, and 60 kGy spectra for clarity. All presented XAS spectra (besides E_0) are renormalized "pure" species, in which any remaining E_0 component (as determined by EPR, see supplementary information) has been subtracted from the experimentally observed spectrum. Prior to any spectra subtractions an 11-point boxcar average smoothing was applied.

Following cryoreduction, only minor increases in the intensity of the white line region from 7125-7135 eV is observed, approximately 1.2-2% of the total normalized intensity (Figure S8). While this is only a small degree of change, we can approximate whether such a shift is relevant based upon previously reported Fe Kα-HERFD spectra of FeS clusters, such as the difference between the $[MoFe_3S_4]^{3+}$ and $[VFe_3S_4]^{2+}$ cubanes which differ by one electron at Fe (Figure S17). In these cubanes, an increase of approximately 6% normalized intensity is found at the white line for the more Fe-reduced $[VFe_3S_4]^{2+}$ cubane, which arises from the addition a single electron over the

three observed Fe centers. Meanwhile, a difference of ~7% white line intensity has also been found between the P^{1+} and P^{N} states of the P-cluster (Figure S20),[14] a 5% increase in $[Et_4N]_n[LFe_2S_2]^{n-}$ (between n = 2 and 3) (Figure S19),[15] and 10% between the VFe and MoFe proteins (Figure S18),[10] although recent crystallographic studies have shown additional light atom coordination in the resting state of FeVco relative to FeMoco which may complicate the interpretation of this feature.[16]

Roughly equating the white line change observed between $[MoFe_3S_4]^{3+}$ and $[VFe_3S_4]^{2+}$ to the MoFe system requires accounting for the 15 Fe present between the FeMoco and P-clusters, and therefore only an increase of ~1.2% would then be anticipated in the protein. Performing the same exercise with the other systems from Figures S17-S20, we can calculate a range of possible white-line increases from ~0.5-10%, all of which would still match an Fe-centered reduction. With these considerations, the small magnitude of the observed changes in the cryoreduced/annealed series is not surprising, and still consistent with an Fe based reduction.

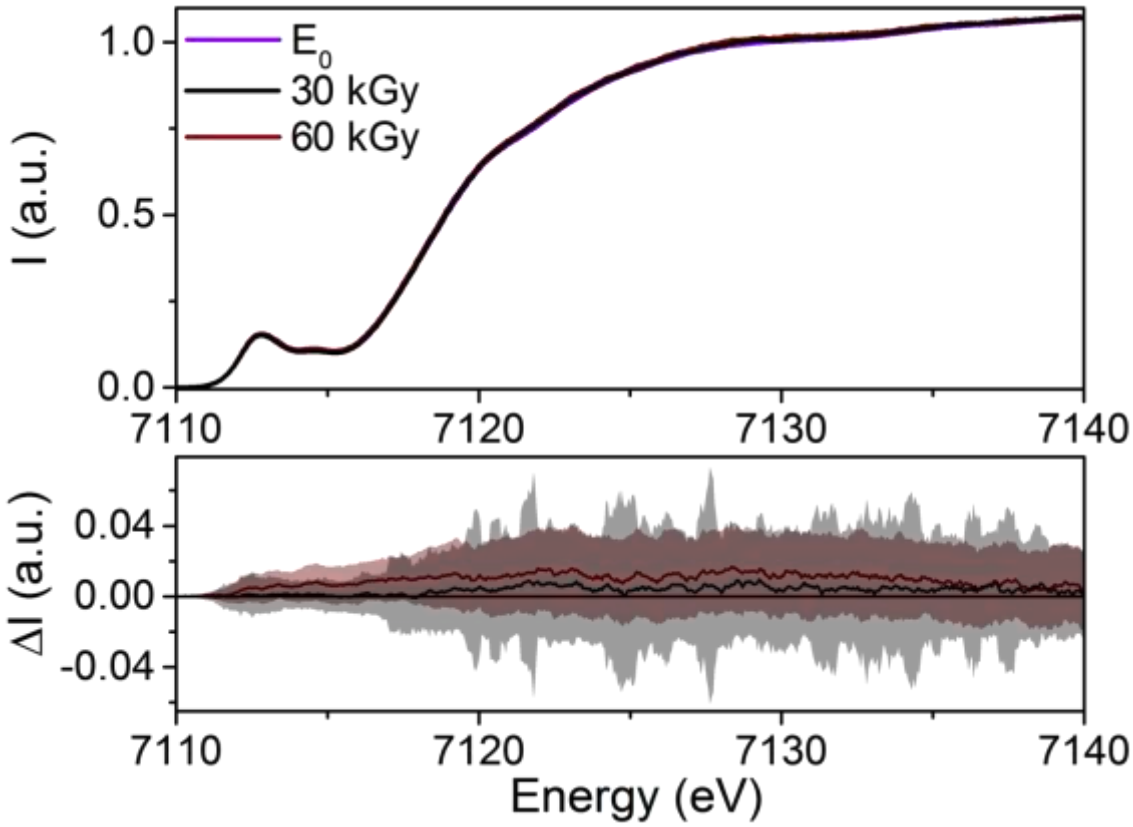

Figure S9. (top) Comparison of the E_0, 30 kGy reduced, and 60 kGy reduced Fe Kα-HERFD spectra. (bottom) Difference spectra of (black) 30 kGy – E_0 and (wine) 60 kGy – E_0, with standard deviations.

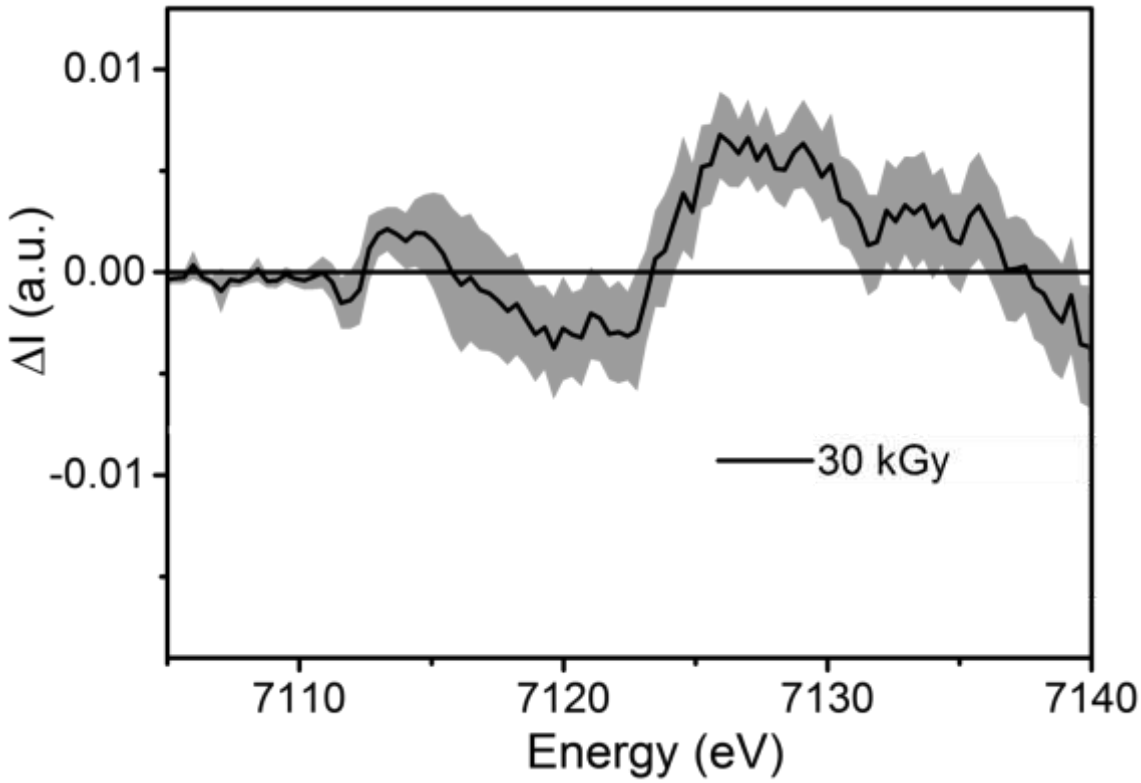

Figure S10. Difference spectrum generated by subtracting the Fe K-edge PFY spectrum of E_0 from that of 30 kGy. Standard deviation is shown as the partially transparent complimenting color.

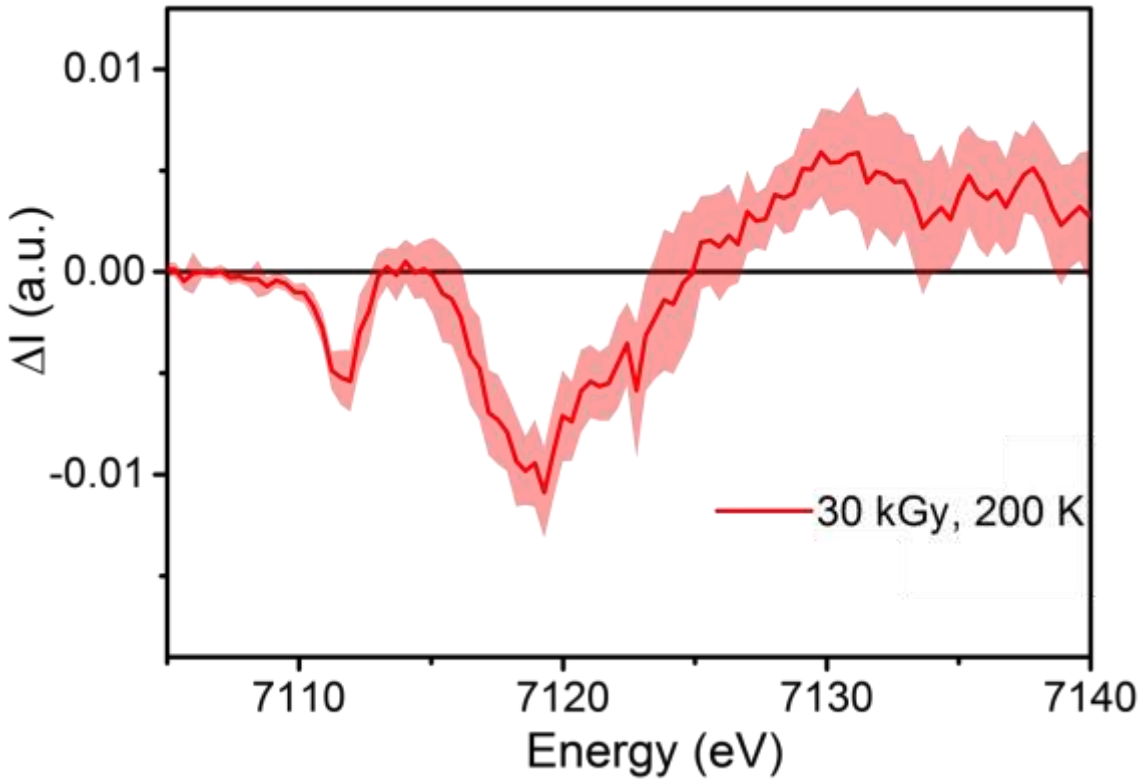

Figure S11. Difference spectrum generated by subtracting the Fe K-edge PFY spectrum of E_0 from that of 30 kGy, 200 K. Standard deviation is shown as the partially transparent complimenting color.

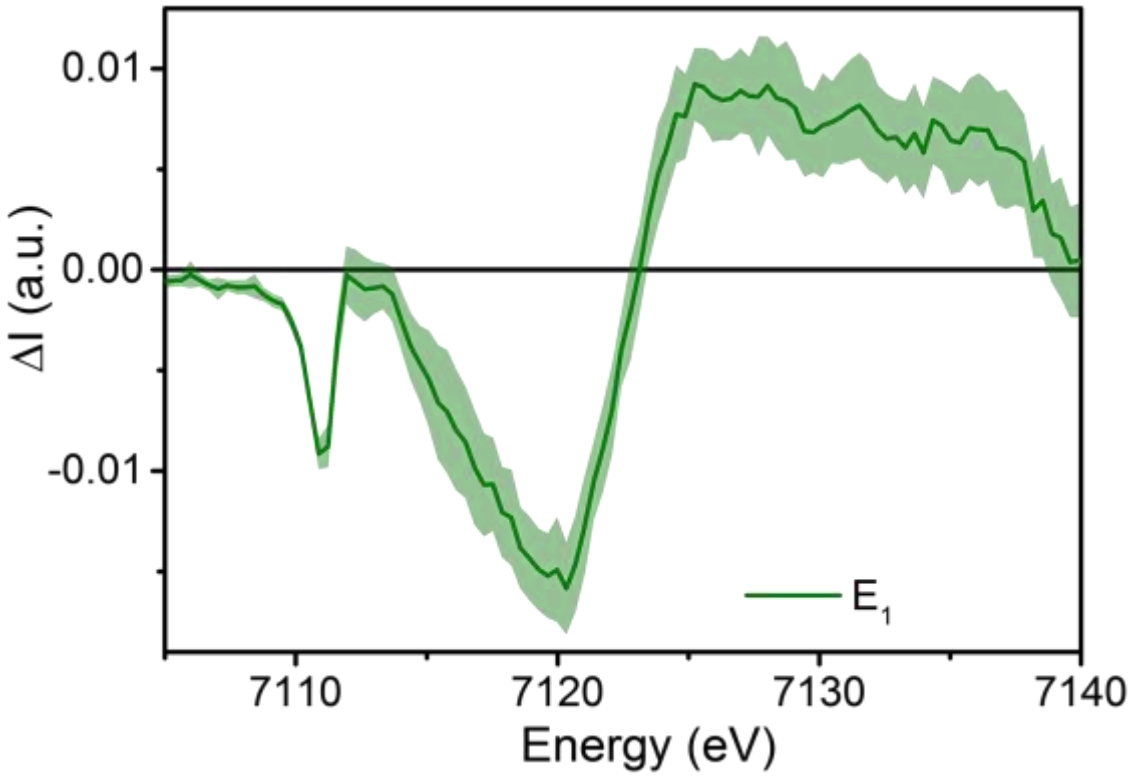

Figure S12. Difference spectrum generated by subtracting the Fe K-edge PFY spectrum of E_0 from that of E_1. Standard deviation is shown as the partially transparent complimenting color.

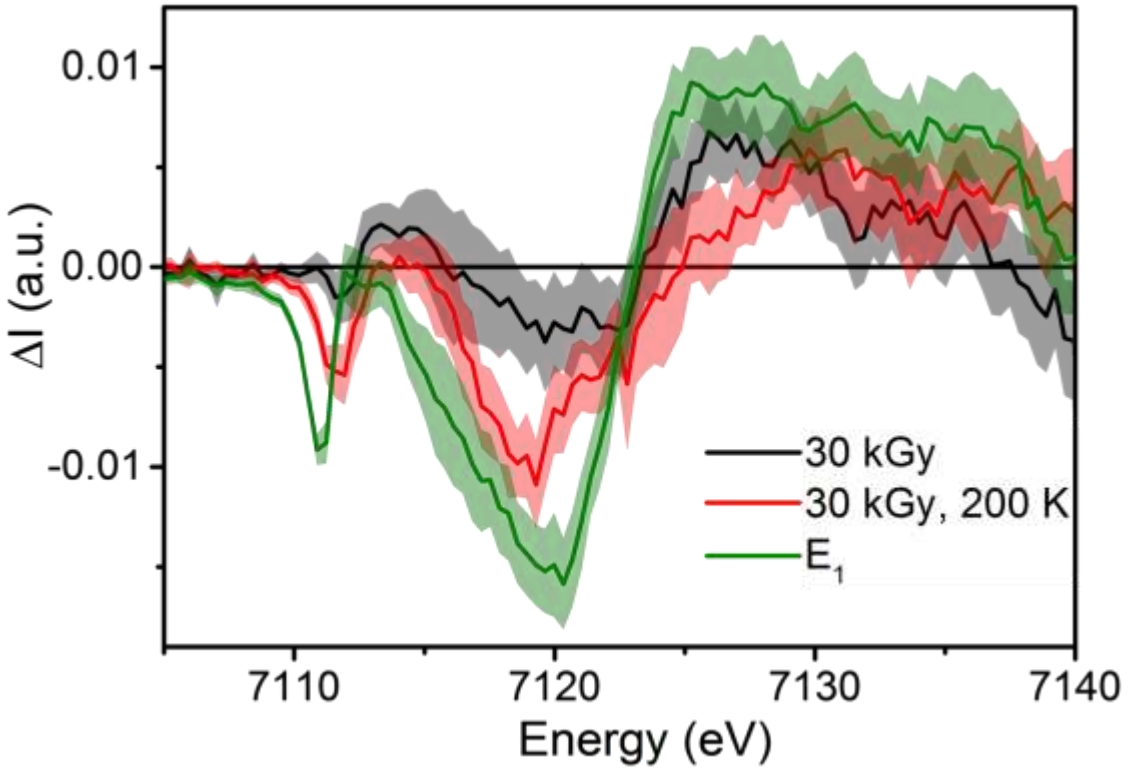

Figure S13. Comparison of the difference spectra generated by subtracting the Fe K-edge PFY spectrum of E_0 from the spectra of E_1 (green), 30 kGy, 200 K (red), and 30 kGy (black). Standard deviations are shown as the partially transparent complimenting color.

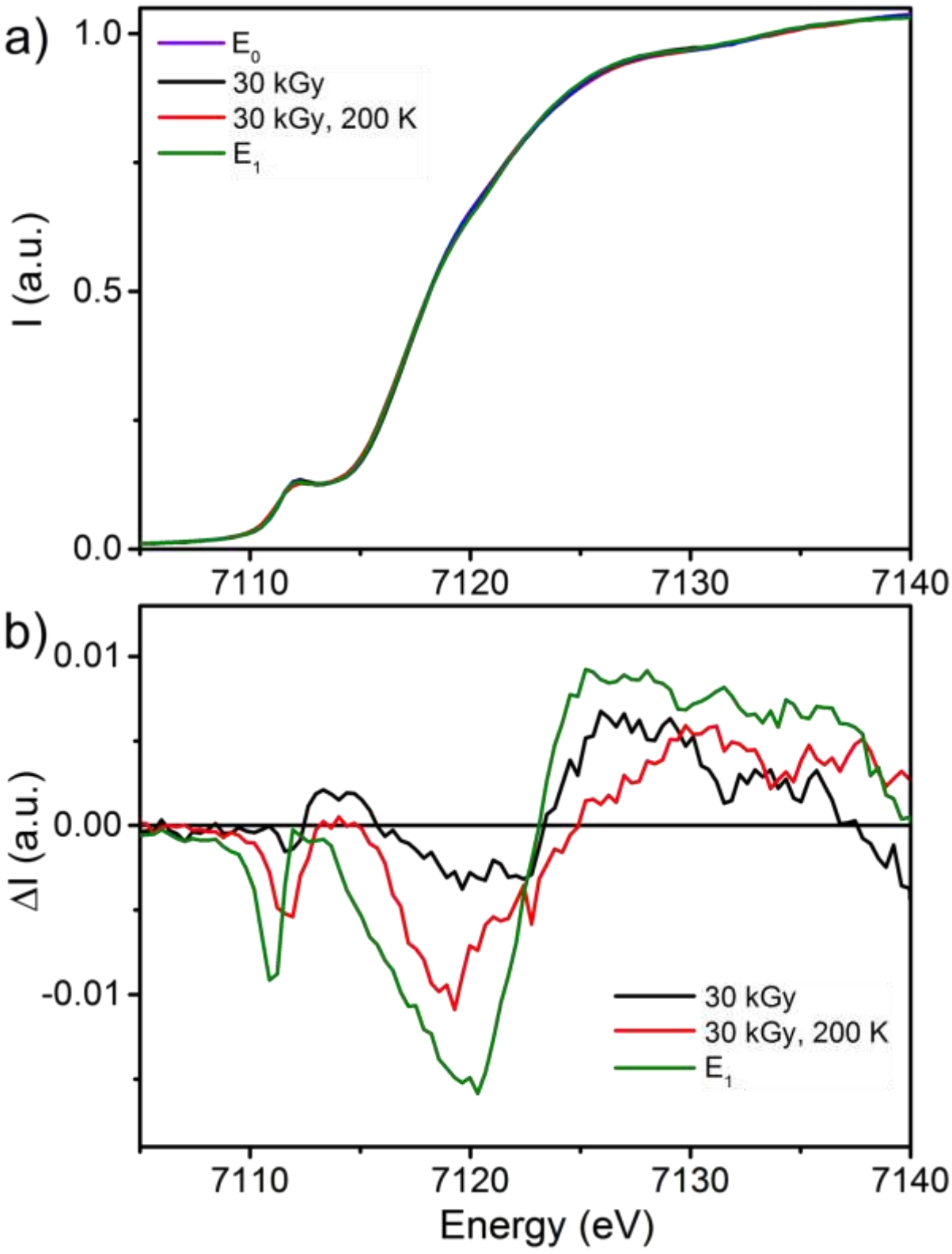

Figure S14. Enlarged version of Figure 5 from the main text. Comparison of the difference spectra generated by subtracting the Fe K-edge XAS spectrum of E_0 from the spectra of E_1 (green), 30 kGy, 200 K (red), 30 kGy, 235 K (blue), and 30 kGy (black).

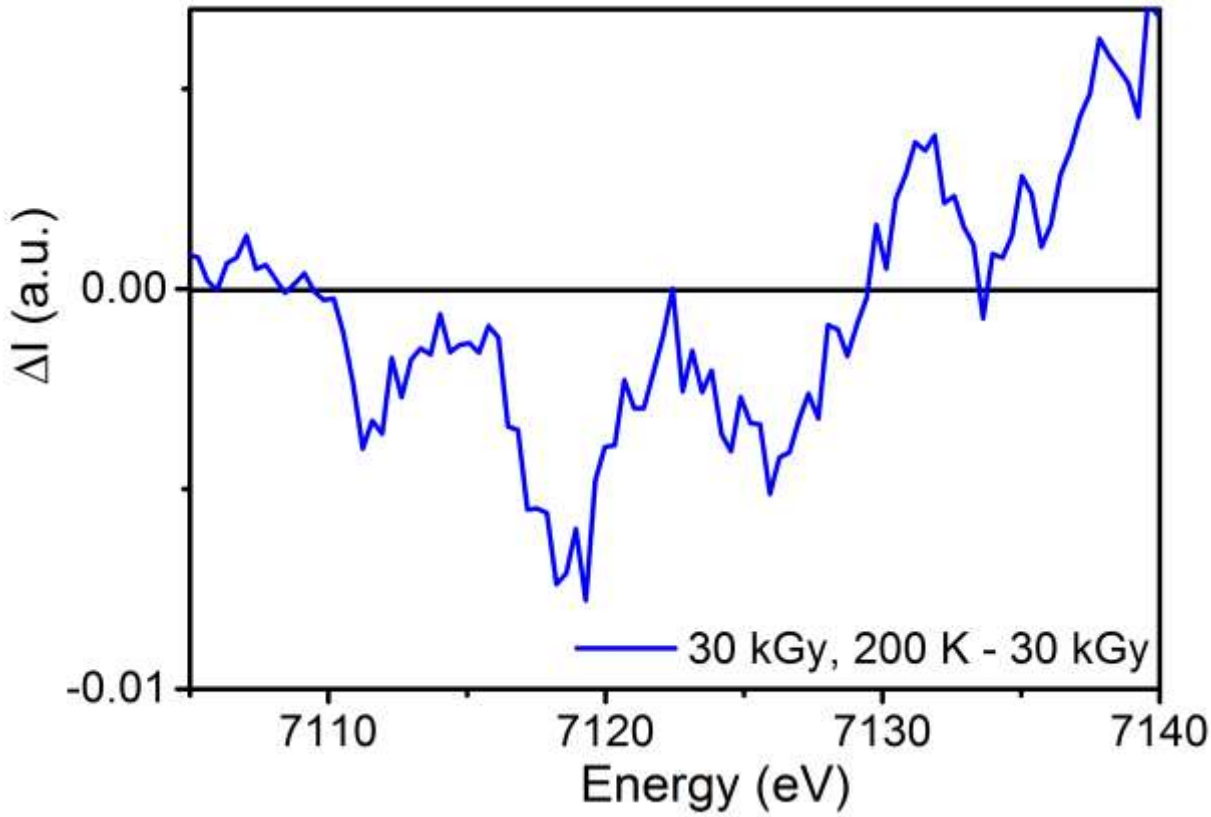

Figure S15. Difference spectrum of 30 kGy, 200 K – 30 kGy to illustrate the changes observed upon annealing of the cryoreduced.

S5. Comparisons of multiple oxidation states in FeS clusters using Fe XAS

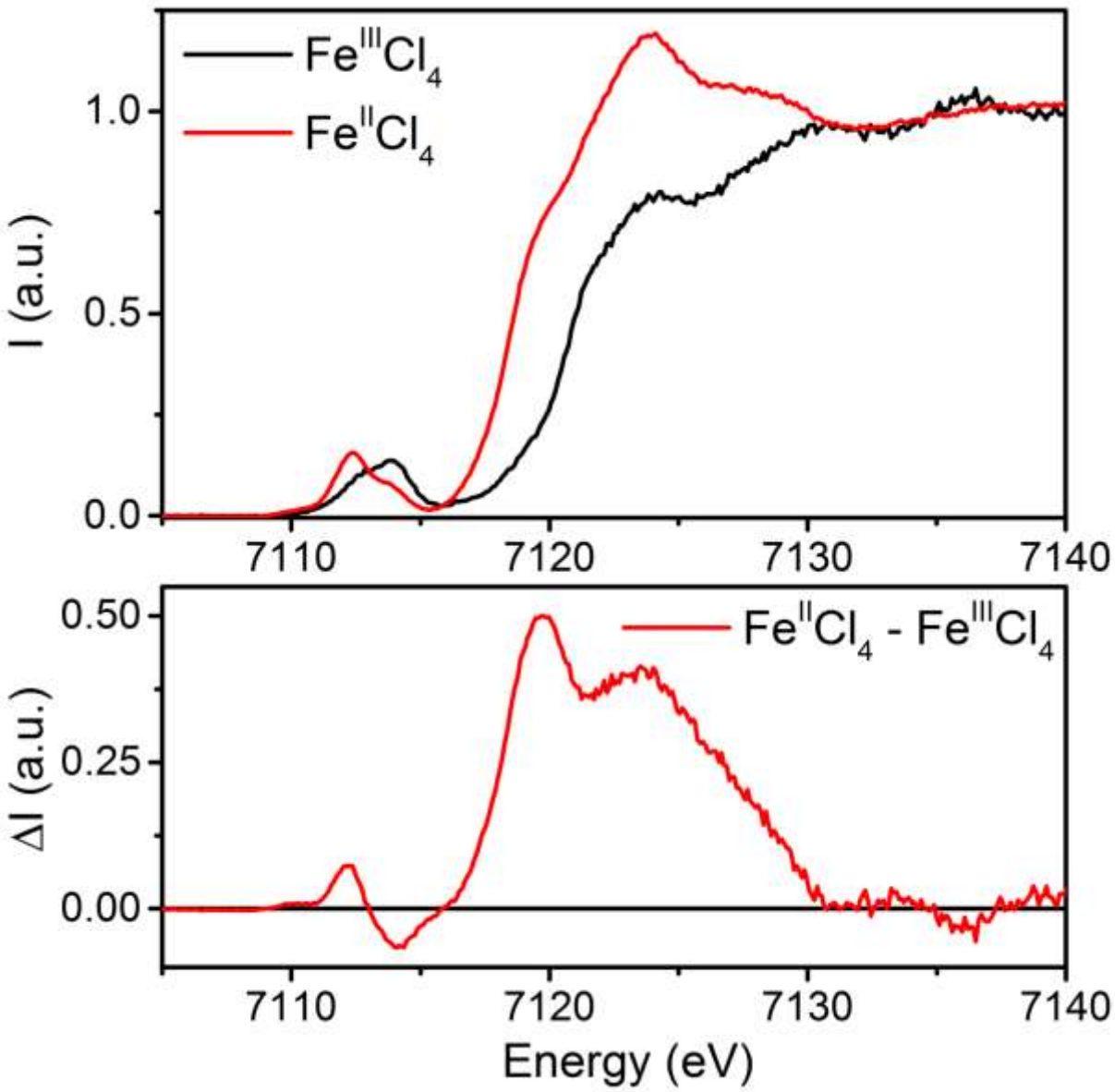

Figure S16. (top) Comparison of the Fe Kβ-HERFD XAS of $Fe^{III}Cl_4$ (black) and $Fe^{II}Cl_4$ (red). (bottom) Difference spectrum generated by subtracting the spectrum of $Fe^{III}Cl_4$ from the spectrum of $Fe^{II}Cl_4$.

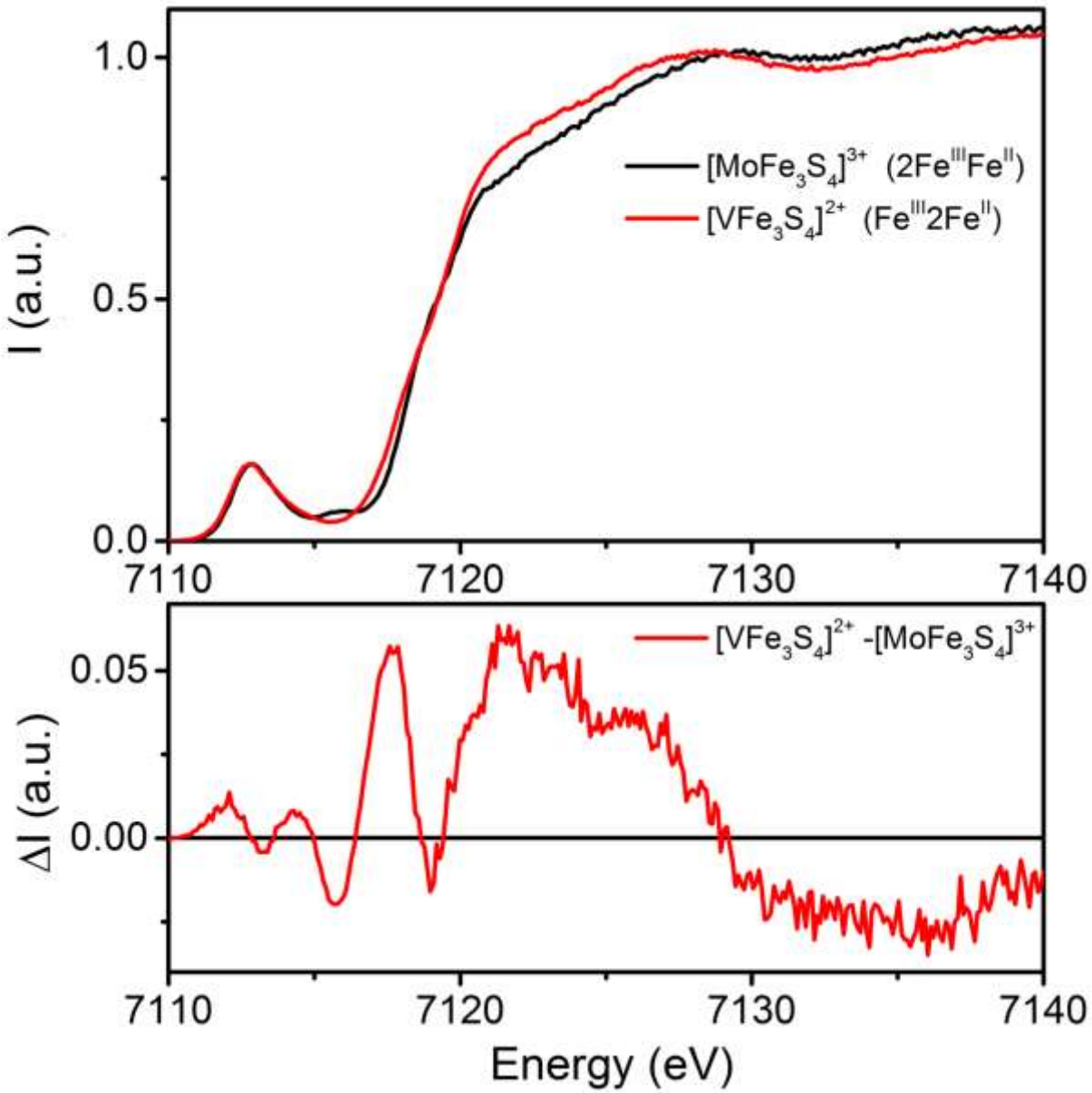

Figure S17. (top) Comparison of the Fe Kα-HERFD XAS of the $[Et_4N][TpMo^{III}Fe_3S_4Cl_3]$ and $[Me_4N][TpV^{III}Fe_3S_4Cl_3]$ cubanes. Reproduced with permission from reference 10.[10] Copyright 2017, Royal Society of Chemistry. (bottom) Difference spectrum generated by subtracting the spectrum of $[Et_4N][TpMo^{III}Fe_3S_4Cl_3]$ from the spectrum of $[Me_4N][TpV^{III}Fe_3S_4Cl_3]$.

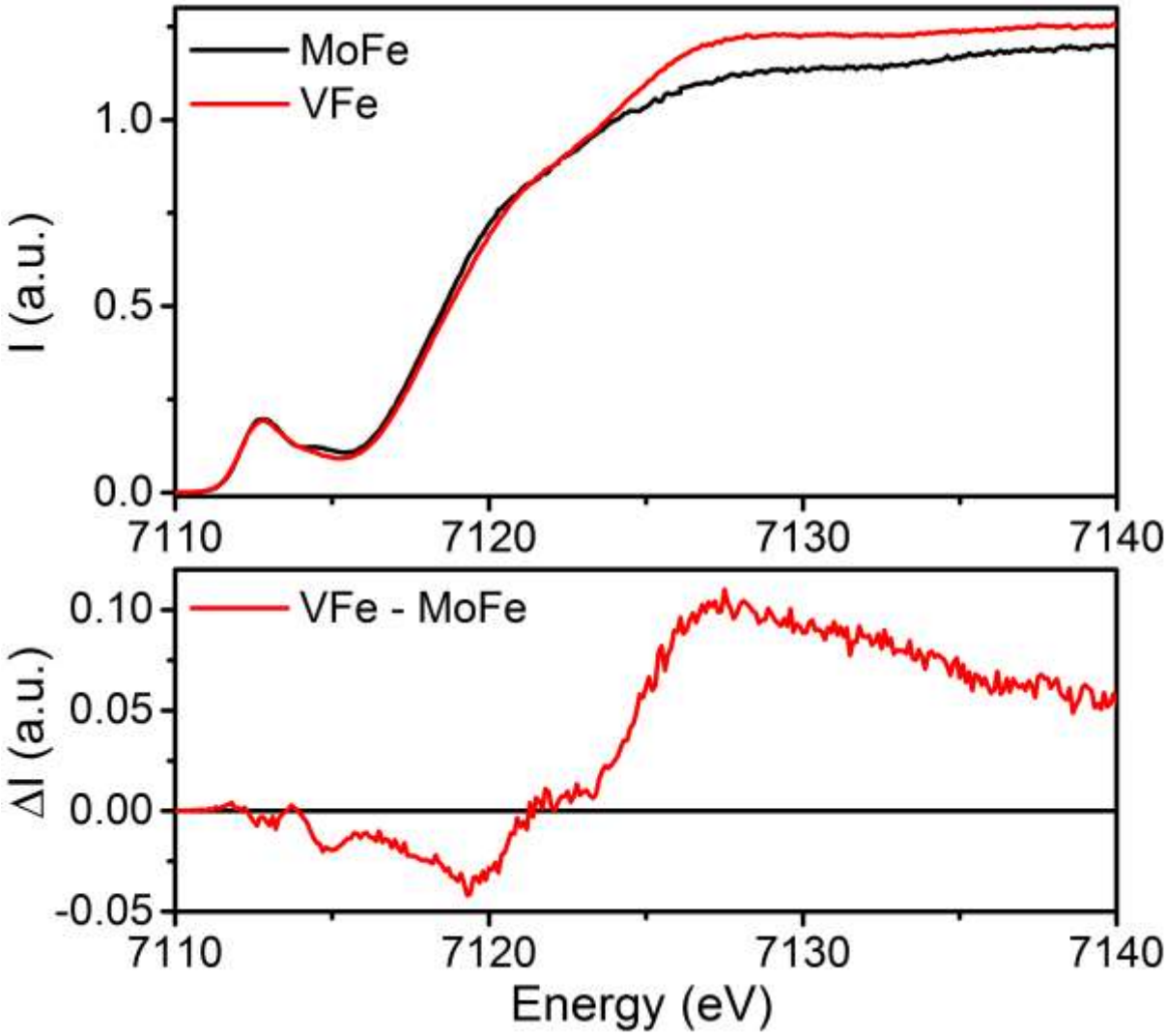

Figure S18. (top) Comparison of the Fe Kα-HERFD XAS of MoFe (black) and VFe (red). Reproduced with permission from reference 10.[10] Copyright 2017, Royal Society of Chemistry. (bottom) Difference spectrum generated by subtracting the spectrum of MoFe from the spectrum of VFe.

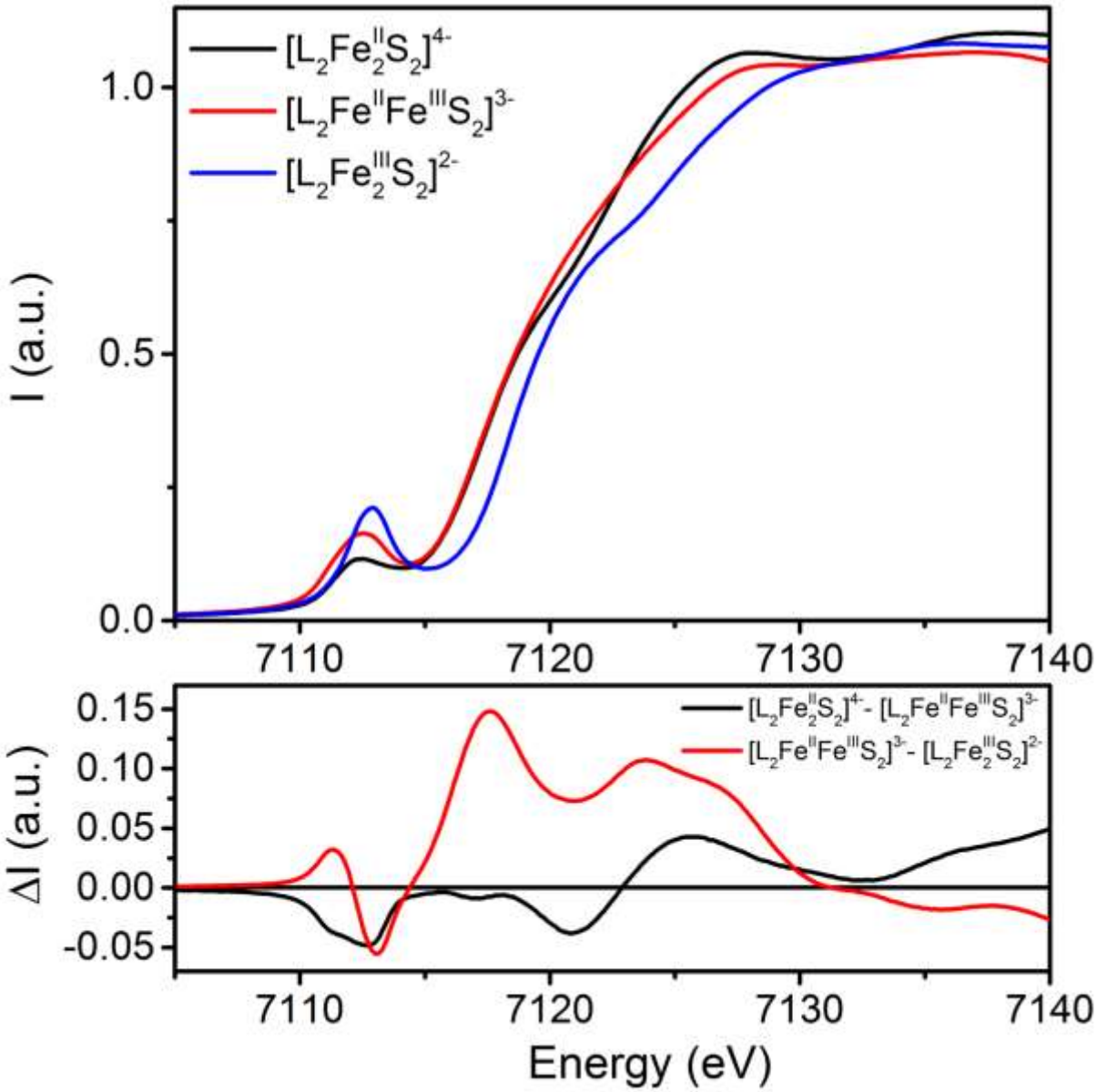

Figure S19. (top) Comparison of the Fe PFY-XAS of the series $[Et_4N]_n[LFe_2S_2]^{n-}$, n = 2, 3, 4. Reproduced with permission from reference 15.[15] Copyright 2016, American Chemical Society. (bottom) Difference spectra generated by subtracting the spectrum of $[Et_4N]_3[LFe_2S_2]^{3-}$ from $[Et_4N]_4[LFe_2S_2]^{4-}$ (black), and $[Et_4N]_2[LFe_2S_2]^{2-}$ from $[Et_4N]_3[LFe_2S_2]^{3-}$ (red).

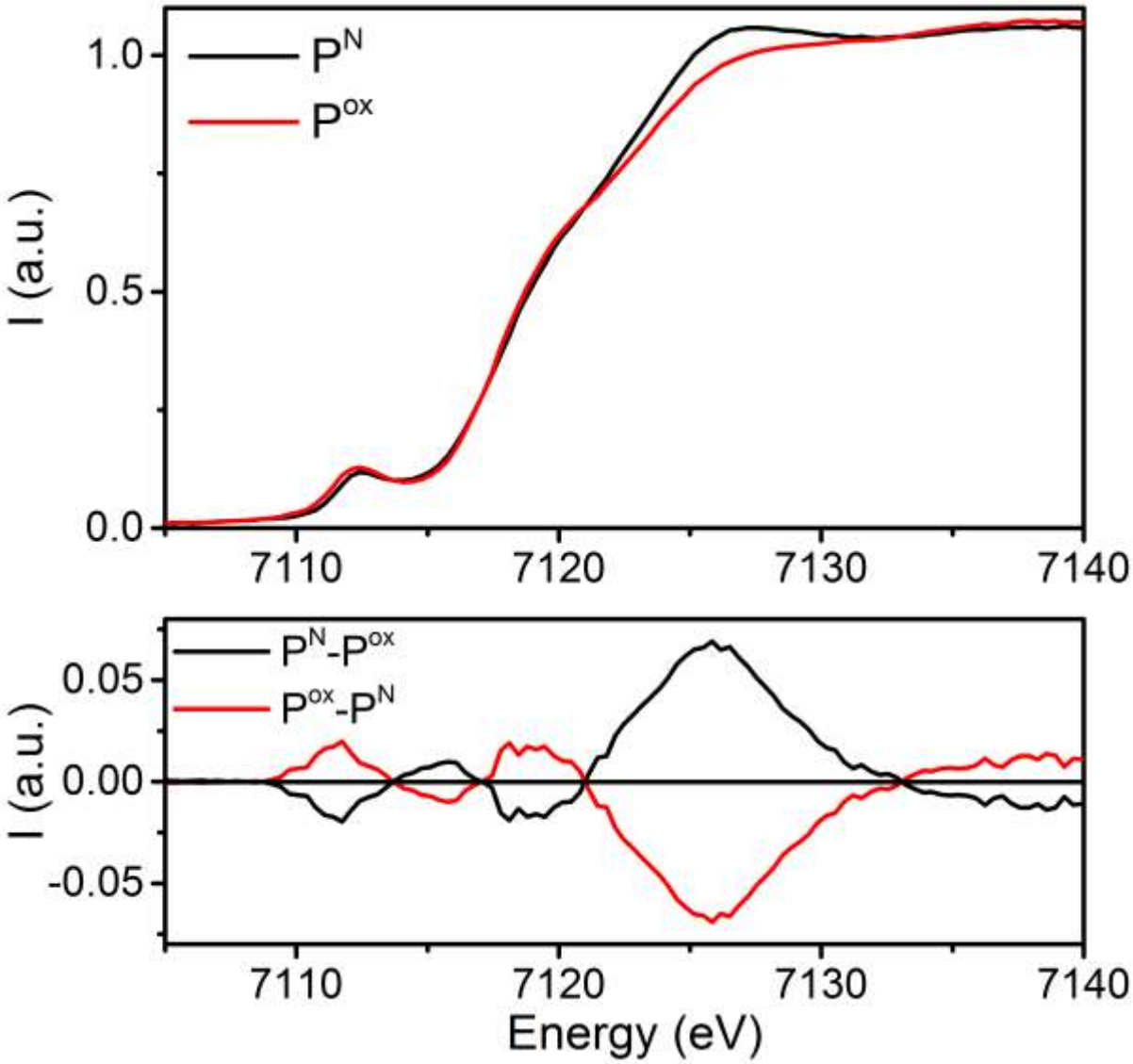

Figure S20. (top) Digitized and splined spectra of P^N and P^{ox} from reference 14.[14] (bottom) Difference spectra generated by subtraction of P^{ox} from P^N (black), and likewise P^N from P^{ox} (red). Reproduced with permission from reference 14. Copyright 1998, Springer Nature.

S6. ^{57}Fe Mössbauer

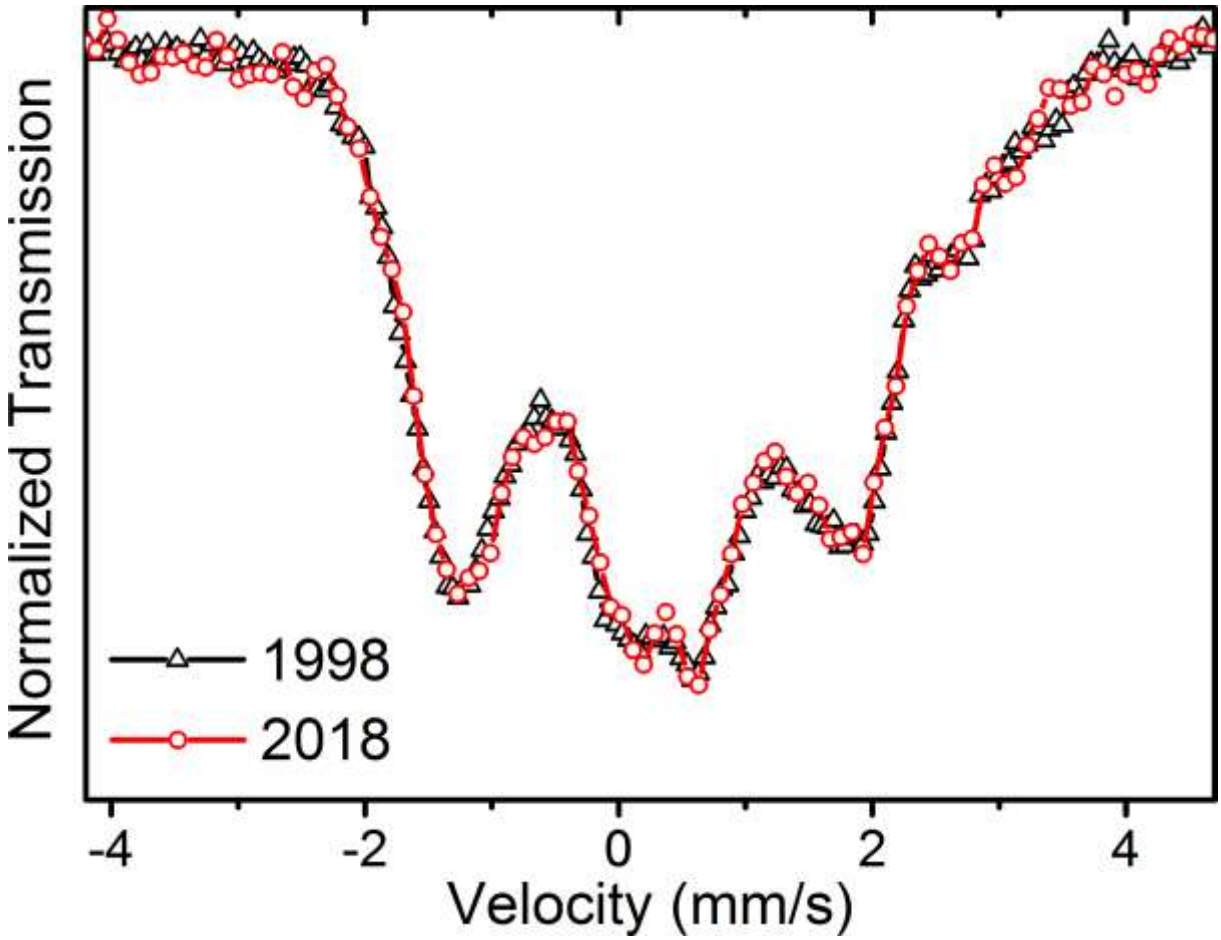

Figure S21. Comparison of the 4.2 K, 0.45 T ^{57}Fe Mössbauer spectra of resting (E_0) Mo N2ase sample containing selectively ^{57}Fe enriched FeMoco acquired in 1998[5] (black) and later in 2018 (red). This sample was stored at consistent cryogenic temperatures (~77 K) over this 20 year time period, and is the same as that used in all present measurements.

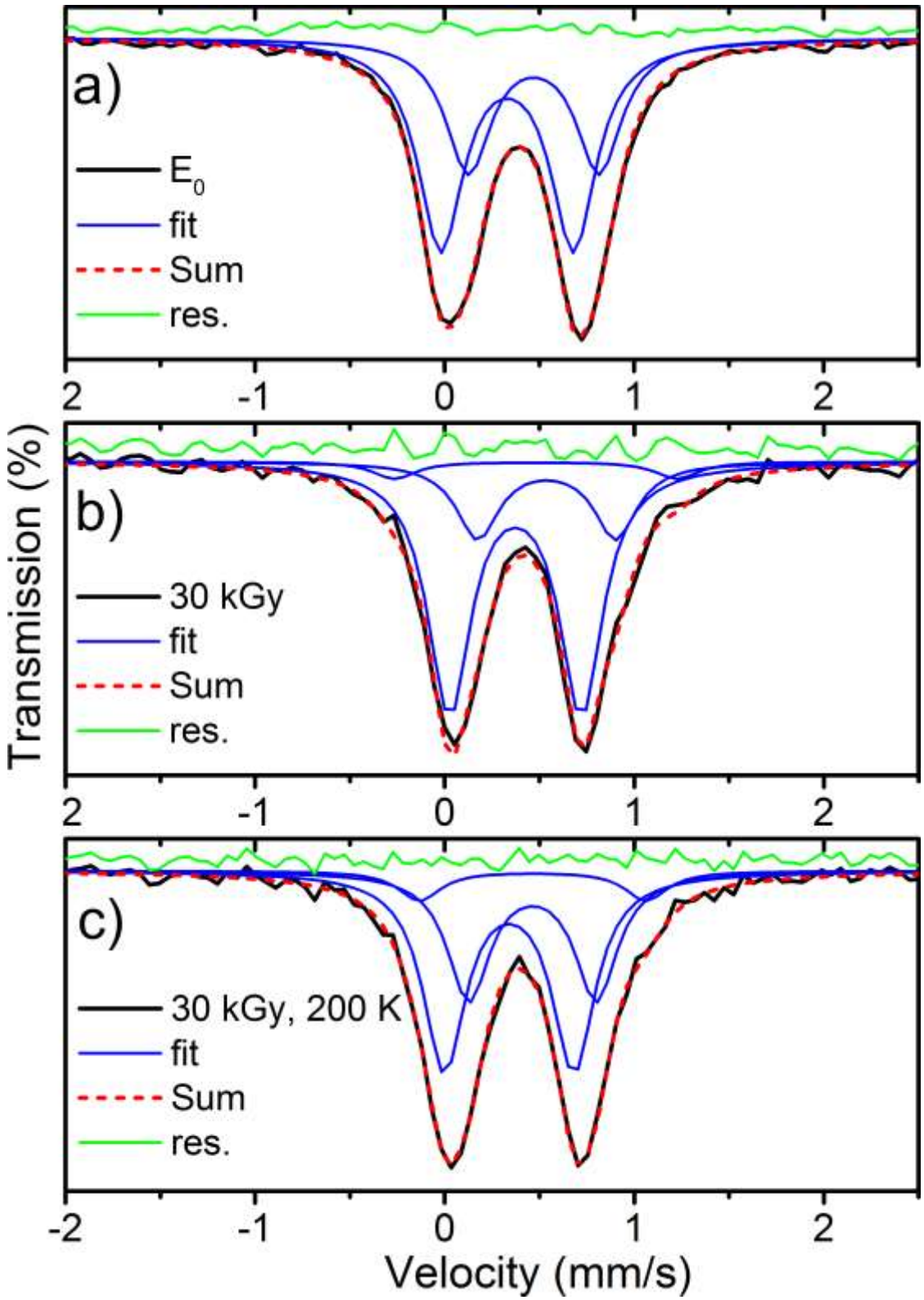

Figure S22. Fits of the a) resting E_0, b) 30 kGy, and c) 30 kGy, 200 K ^{57}Fe Mössbauer spectra of a selectively ^{57}FeMoco/^{56}P-cluster enriched MoFe sample. Based on the EPR data collected for the XAS samples, the 30 kGy and 30 kGy, 200 K spectra contain ~60% E_0. The spectra were collected under the following conditions: E_0 (100 K, 0 T), 30 kGy (90 K, 0.1 T), and 30 kGy, 200 K (90 K, 0 T). The experimental error is included on the fit residual (green), < 2% of the total absorption in all three experiments.

Table S3. Summary of ^{57}Fe Mössbauer fits of E_0, 30 kGy, and 30 kGy, 200 K samples. The average isomer shift of each species is formulated by the weighted average of the isomer shifts of its individual components. Linewidths were held constant at 0.3 mm/s in all fits. *calculated by subtraction of $\delta(E_0)$. **adjusted for the presence of 60% E_0 by multiplying $\Delta\delta_{avg}$ by 2.5. Fits were performed using linewidths of 0.29[a] and 0.27[b] mm/s. The spectra were collected under the following conditions: E_0 (100 K, 0 T), 30 kGy (90 K, 0.1 T), and 30 kGy, 200 K (90 K, 0 T).

	E_0[a]			30 kGy[b]			30 kGy, 200 K[a]		
Component	δ	ΔE_Q	%	δ	ΔE_Q	%	δ	ΔE_Q	%
1	0.33	0.70	61	0.37	0.70	73	0.34	0.68	57
2	0.47	0.69	39	0.54	0.73	22	0.46	0.67	35
3				0.48	1.49	5	0.46	1.2	8
average	0.38			0.41			0.39		
$\Delta\delta_{avg}$*				0.03			0.01		
$\Delta\delta_{avg}$**				0.07			0.02		

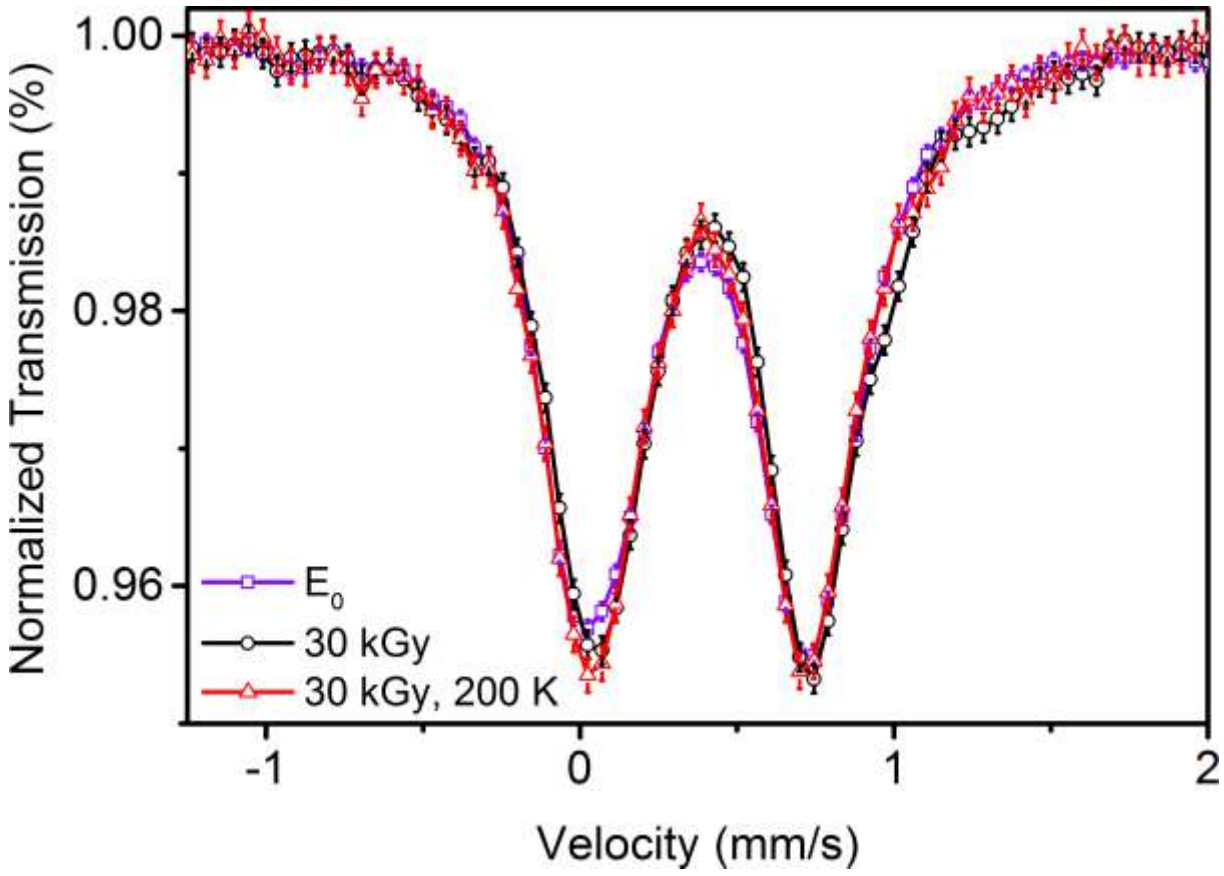

Figure S23. Comparison of the experimental resting E_0 (violet), 30 kGy (black), and 30 kGy, 200 K (red) ^{57}Fe Mössbauer spectra of a selectively ^{57}FeMoco/^{56}P-cluster enriched MoFe sample. Based on EPR, the 30 kGy and 30 kGy, 200 K spectra contain ~60% E_0. The spectra were collected under the following conditions: E_0 (100 K, 0 T), 30 kGy (90 K, 0.1 T), and 30 kGy, 200 K (90 K, 0 T). Error bars are provided based on a Poisson distribution.

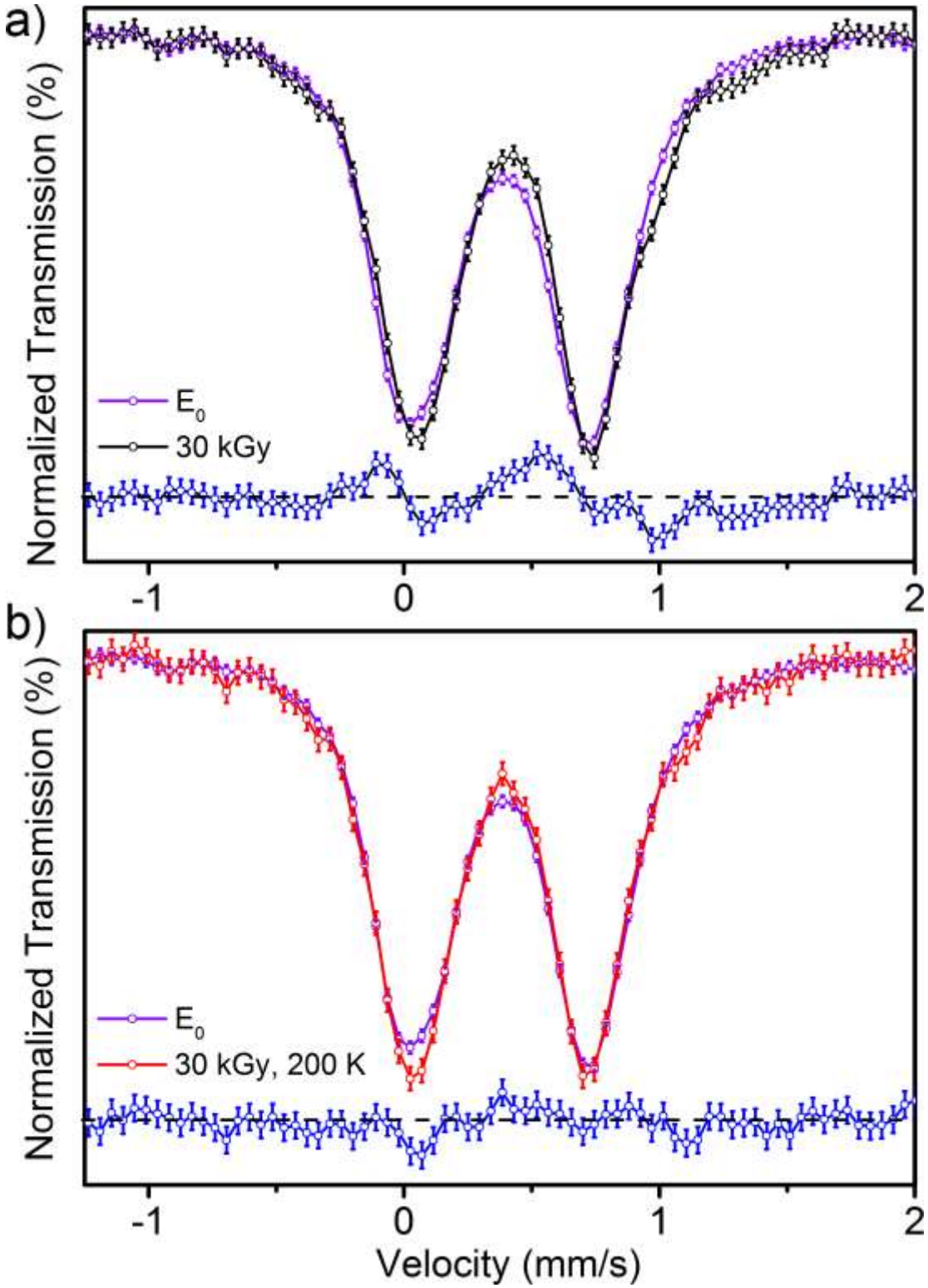

Figure S24. Comparison of the a) 30 kGy (black), and b) 30 kGy, 200 K (red) ^{57}Fe Mössbauer spectra with that of the resting E_0 (violet) state. Measurements were performed on a selectively ^{57}FeMoco/^{56}P-cluster enriched MoFe sample. Based on EPR, the 30 kGy and 30 kGy, 200 K spectra contain ~60% E_0. The spectra were collected under the following conditions: E_0 (100 K, 0 T), 30 kGy (90 K, 0.1 T), and 30 kGy, 200 K (90 K, 0 T). Difference spectra of a) 30 kGy – E_0 and b) 30 kGy, 200 K – E_0 are provided as a blue line at the bottom of their respective plots, with the dashed black line representing the zero. Error bars are provided based on a Poisson distribution.

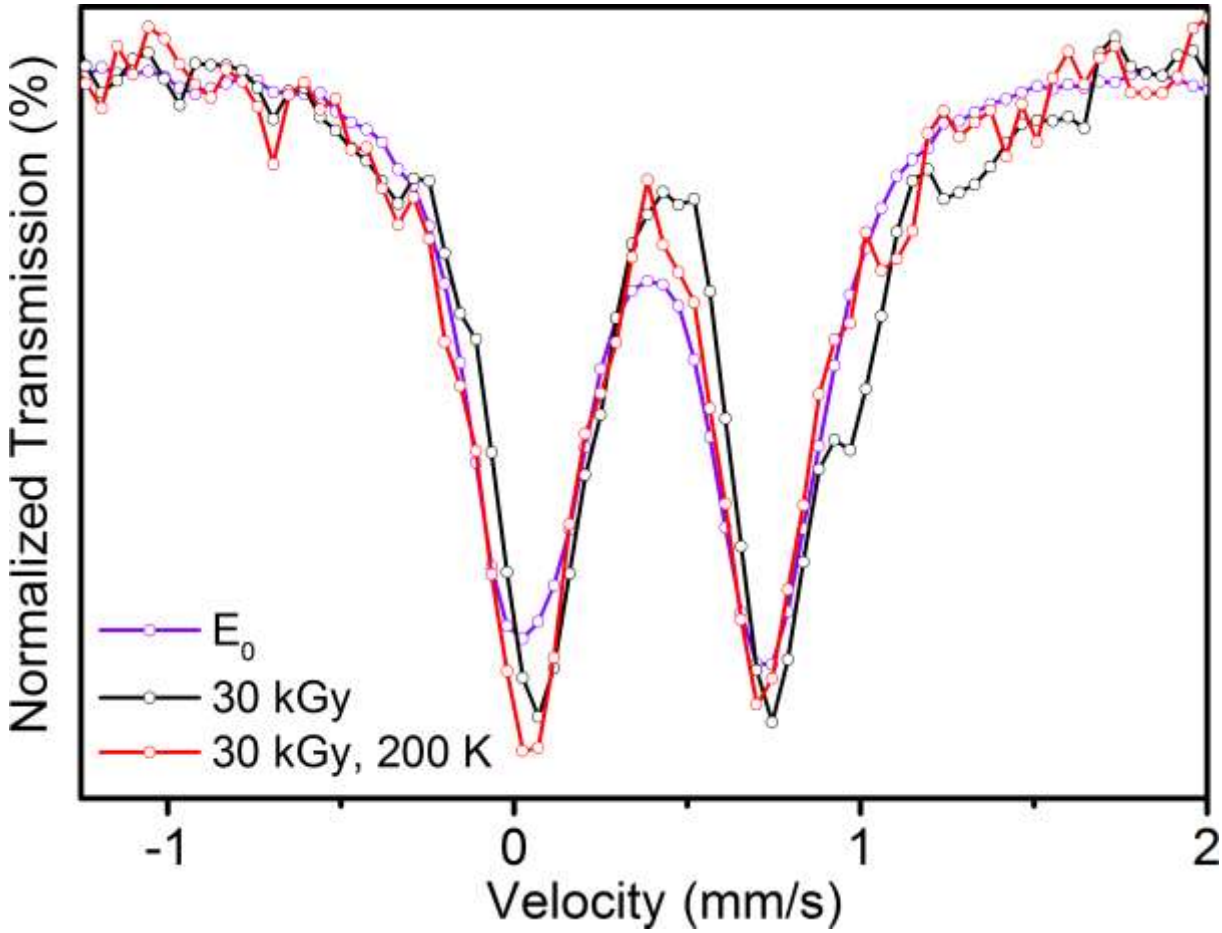

Figure S25. Comparison of the renormalized "**pure**" ^{57}Fe Mössbauer spectra of the 30 kGy (black) and 30 kGy, 200 K (red) samples with that of the resting E_0 (violet) state. Measurements were performed on a selectively ^{57}FeMoco/^{56}P-cluster enriched MoFe sample. The presented 30 kGy and 30 kGy, 200 K spectra were generated by subtraction of the E_0 component (~60% based on EPR) from the measured spectra, followed by renormalization. The spectra were collected under the following conditions: E_0 (100 K, 0 T), 30 kGy (90 K, 0.1 T), and 30 kGy, 200 K (90 K, 0 T).

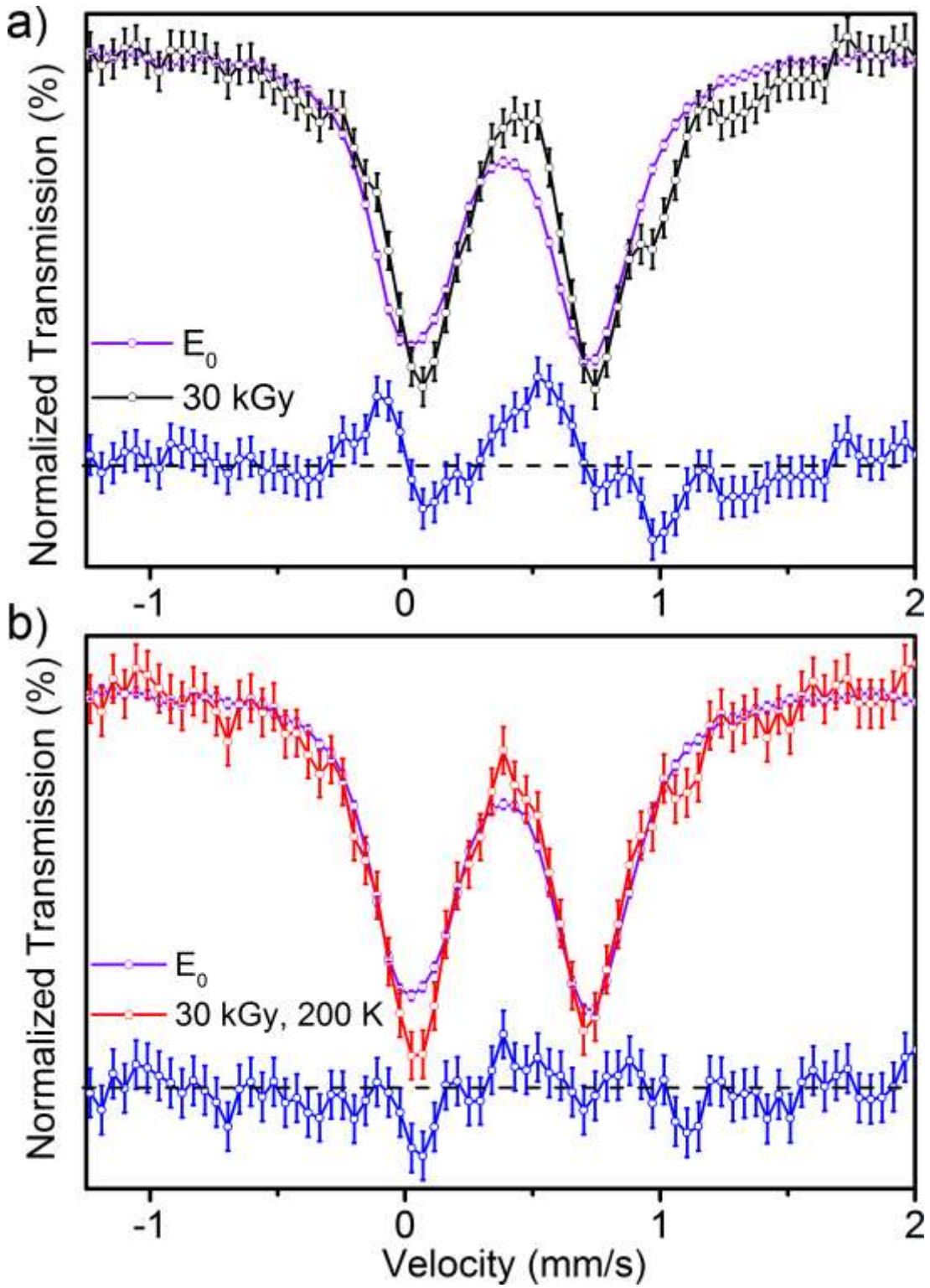

Figure S26. Comparison of the a) 30 kGy (black), and b) 30 kGy, 200 K (red) ^{57}Fe Mössbauer spectra with that of the resting E_0 (violet) state. Measurements were performed on a selectively ^{57}FeMoco/^{56}P-cluster enriched MoFe sample. The presented 30 kGy and 30 kGy, 200 K spectra were generated by subtraction of the E_0 component (~60% based on EPR) from the measured spectra, followed by renormalization. The spectra were collected under the following conditions: E_0 (100 K, 0 T), 30 kGy (90 K, 0.1 T), and 30 kGy, 200 K (90 K, 0 T). Difference spectra of a) 30 kGy – E_0 and b) 30 kGy, 200 K – E_0 are provided as a blue line at the bottom of their respective plots, with the dashed black line representing the zero. Error bars are provided based on a Poisson distribution.

References

1. Dilworth, J. R.; Zubieta, J. A. Preparation and Crystal-Structure of [Mo{$S_2P(OMe)_2$}$_3$] and an Improved Route to [$MoCl_3(thf)_3$]. *J. Chem. Soc., Dalton Trans.* **1983,** 397-398.
2. Stoffelbach, F.; Saurenz, D.; Poli, R. Improved Preparations of Molybdenum Coordination Compounds from Tetrachlorobis(diethyl ether)molybdenum(IV). *Eur. J. Inorg. Chem.* **2001,** *10*, 2699-2703.
3. Kowalska, J. K.; Henthorn, J. T.; Van Stappen, C.; Trncik, C.; Einsle, O.; Keavney, D.; DeBeer, S. X-ray Magnetic Circular Dichroism Spectroscopy Applied to Nitrogenase and Related Models: Experimental Evidence for a Spin-Coupled Mo(III). *Angew. Chem., Int. Ed.* **2019**, DOI: 0.1002/anie.201901899.
4. Tittsworth, R. C.; Hales, B. J., Detection of EPR Signals Assigned to the 1-equiv-Oxidized P-Clusters of the Nitrogenase MoFe-Protein from Azotobacter-Vinelandii. *J. Am. Chem. Soc.* **1993,** *115*, 9763-9767.
5. Yoo, S. J.; Angove, H. C.; Papaefthymiou, V.; Burgess, B. K.; Münck, E., Mössbauer Study of the MoFe Protein of Nitrogenase from Azotobacter vinelandii Using Selective ^{57}Fe Enrichment of the M-Centers. *J. Am. Chem. Soc.* **2000,** *122*, 4926-4936.
6. Aasa, R.; Vänngård, T. EPR Signal Intensity and Powder Shapes: A Reexamination. *J. Magn. Reson.* **1975,** *19*, 308-315.
7. Bjornsson, R.; Lima, F. A.; Spatzal, T.; Weyhermuller, T.; Glatzel, P.; Bill, E.; Einsle, O.; Neese, F.; DeBeer, S. Identification of a spin-coupled Mo(III) in the nitrogenase iron-molybdenum cofactor. *Chem. Sci.* **2014,** *5*, 3096-3103.
8. DeBeer George, S.; Brant, P.; Solomon, E. I. Metal and Ligand K-Edge XAS of Organotitanium Complexes: Metal 4p and 3d Contributions to Pre-edge Intensity and Their Contributions to Bonding. *J. Am. Chem. Soc.* **2005,** *127*, 667-674.
9. Lima, F. A.; Bjornsson, R.; Weyhermüller, T.; Chandrasekaran, P.; Glatzel, P.; Neese, F.; DeBeer, S. High-resolution molybdenum K-edge X-ray absorption spectroscopy analyzed with time-dependent density functional theory. *Phys. Chem. Chem. Phys.* **2013,** *15*, 20911-20.
10. Rees, J. A.; Bjornsson, R.; Kowalska, J. K.; Lima, F. A.; Schlesier, J.; Sippel, D.; Weyhermüller, T.; Einsle, O.; Kovacs, J. A.; DeBeer, S. Comparative electronic structures of nitrogenase FeMoco and FeVco. *Dalton Trans.* **2017,** *46*, 2445-2455.
11. Westre, T. E.; Kennepohl, P.; DeWitt, J. G.; Hedman, B.; Hodgson, K. O.; Solomon, E. I. A Multiplet Analysis of Fe K-Edge 1s → 3d Pre-Edge Features of Iron Complexes. *J. Am. Chem. Soc.* **1997,** *119*, 6297-6314.
12. Shulman, R. G.; Yafet, Y.; Eisenberger, P.; Blumberg, W. E. Observations and interpretation of x-ray absorption edges in iron compounds and proteins. *Proc. Nat. Acad. Sci. U.S.A.* **1976,** *73*, 1384-1388.
13. Yao, S.; Meier, F.; Lindenmaier, N.; Rudolph, R.; Blom, B.; Adelhardt, M.; Sutter, J.; Mebs, S.; Haumann, M.; Meyer, K.; Kaupp, M.; Driess, M. Biomimetic [2Fe-2S] Clusters with Extensively Delocalized Mixed-Valence Iron Centers. *Angew. Chem., Int. Ed. Engl.* **2015,** *54*, 12506-10.
14. Musgrave, K. B.; Liu, H. I.; Ma, L.; Burgess, B. K.; Watt, G.; Hedman, B.; Hodgson, K. O. EXAFS studies on the P^N and P^{OX} states of the P-clusters in nitrogenase. *JBIC, J. Biol. Inorg. Chem.* **1998,** *3*, 344-352.
15. Kowalska, J. K.; Hahn, A. W.; Albers, A.; Schiewer, C. E.; Bjornsson, R.; Lima, F. A.; Meyer, F.; DeBeer, S. X-ray Absorption and Emission Spectroscopic Studies of $[L_2Fe_2S_2]^n$ Model Complexes: Implications for the Experimental Evaluation of Redox States in Iron-Sulfur Clusters. *Inorg. Chem.* **2016,** *55*, 4485-97.
16. Sippel, D.; Einsle, O. The structure of vanadium nitrogenase reveals an unusual bridging ligand. *Nat. Chem. Biol.* **2017,** *13*, 956-960.